Probing PAC1 receptor activation across species with an engineered sensor

Reto B. Cola[1], Salome N. Niethammer[2], Preethi Rajamannar[3], Andrea Gresch[1], Musadiq A. Bhat[1], Kevin Assoumou[4], Elyse T. Williams[5], Patrick Hauck[5], Nina Hartrampf[5], Dietmar Benke[1,6], Miriam Stoeber[4], Gil Levkowitz[3], Sarah Melzer[2], Tommaso Patriarchi[1,6,*]

[1] Institute of Pharmacology and Toxicology, University of Zürich, Zürich, Switzerland;

[2] Medical University of Vienna, Center for Brain Research, Department for Neuronal Cell Biology, Vienna, Austria

[3] Department of Molecular Neuroscience & Department of Molecular Cell Biology Weizmann Institute of Science, Israel

[4] Department of Cell Physiology and Metabolism, University of Geneva, Geneva, Switzerland;

[5] Department of Chemistry, University of Zürich, Zürich, Switzerland;

[6] Neuroscience Center Zurich, University and ETH Zürich, Zürich, Switzerland;

[*] correspondence to: patriarchi@pharma.uzh.ch

Key words: genetically-encoded sensors, fluorescence, GPCRs, PACAP, PAC1R, Adcyap1, Adcyap1r1, neuropeptide, zebrafish, mouse

Abstract

Class-B1 G protein-coupled receptors (GPCRs) are an important family of clinically relevant drug targets that remain difficult to investigate via high-throughput screening and in animal models. Here, we engineered PAClight1$_{P78A}$, a novel genetically-encoded sensor based on a class-B1 GPCR (the human PAC1 receptor, hmPAC1R) endowed with high dynamic range ($\Delta F/F_0$ = 1100%), excellent ligand selectivity and rapid activation kinetics (τ_{ON} = 1.15 sec). To showcase the utility of this tool for in vitro applications, we thoroughly characterized and compared its expression, brightness and performance between PAClight1$_{P78A}$ transfected and stably-expressing cells. Demonstrating its use in animal models, we show robust expression and fluorescence responses upon exogenous ligand application ex vivo and in vivo in mice, as well as in living zebrafish larvae. Thus, the new GPCR-based sensor can be used for a wide range of applications across the life sciences empowering both basic research and drug development efforts.

Introduction

Class-B1 G protein-coupled receptors (GPCRs) represent an important sub-group of peptide-sensing GPCRs, that are the focus of intense and rapidly-expanding drug development efforts[1,2], driven by extremely successful examples of peptide agonists used in the clinical treatment of metabolic human diseases, such as type-2 diabetes and obesity[3]. One such peptide-GPCR system that has shown growing potential for targetability in the treatment of human disorders is the Pituitary Adenylate Cyclase Activating Peptide (ADCYAP1 or PACAP) and its receptors. PACAP is an endogenous 38-amino acid peptide that is amongst the most phylogenetically-conserved peptides[4]. Its shorter C-terminally-truncated form (i.e. $PACAP_{1-27}$) has 68% homology with the vasoactive-intestinal-peptide (VIP)[5]. In fact, VIP and PACAP share a subfamily of class-B1 G protein-coupled receptors (GPCRs), of which the two receptors VPAC1 and VPAC2 can both be equipotently activated by VIP and PACAP[5]. The third receptor in this subfamily, i.e. the PAC1 receptor (PAC1R, also known as ADCYAP1R1), however, has a reported affinity for PACAP that is 100-1000-fold higher than its affinity to VIP[5]. The tissue distribution of PACAP and its receptors is widespread and they can be found throughout the central and peripheral nervous system, the immune system, in endocrine glands as well as in other organ systems and in many cancerous tissues[5–9]. A large body of evidence has linked the PACAP/PAC1R system to protective functions in the nervous and immune systems, as well as to stress- and anxiety-related behaviors (in particular post-traumatic stress disorder (PTSD)), migraine, nociception, thermoregulation, sleep/wake cycles, and reproductive functions[5,8,10], making it a peptide signaling system of high clinical relevance.

Recently, genetically-encoded GPCR-based sensors have been developed that enable the direct optical detection of GPCR activation by agonist ligands with high sensitivity and spatiotemporal resolution[11–19]. While these tools hold great potential for drug development, pharmacology and neuroscience applications, only a few of them are built from class-B1 peptide-sensing GPCRs[18,20]. Thus, the development of new biosensors based on peptide-sensing GPCRs

62 would greatly benefit the community and serve as a powerful resource for drug screening and life
63 sciences.

64 In this work we engineered PAClight1$_{P78A}$, an ultrasensitive indicator based on the human
65 PAC1 receptor (hmPAC1R). To establish this as a tool for peptide drug screening, we thoroughly
66 characterized its dynamic range, as well as its optical, kinetic, signaling and pharmacological
67 properties in vitro. We further generated stable cell lines and compared them to transfected cells
68 for ligand-induced fluorescence responses using flow cytometry. Additionally, we tested the
69 potential of PAClight1$_{P78A}$ as a tool to study ligand binding and diffusion in animal models. To this
70 end, we examined the sensitivity and specificity of PAClight1$_{P78A}$ in acute mouse brain slices.
71 Moreover, we verified ligand detection in vivo using fiber photometry recording and intracerebral
72 microinfusions in behaving mice.

73 Finally, we demonstrate that the sensor expresses well and produces a large fluorescent
74 response to PACAP$_{1-38}$ following microinjection in the brain of living zebrafish larvae, opening new
75 opportunities for the development and testing of drugs targeting this receptor in the central
76 nervous system.

77 Overall, our new sensor expands the class of genetically-encoded optical tools that can be
78 used for GPCR-targeted HTS assays, reducing the demands on time and costly reagents, and
79 provides new opportunities for functionally testing drugs that target the PAC1R pathway directly
80 in living animals.

81

82

83

84 **Results**

85 **Development of an ultrasensitive PAC1R-based sensor**

86 To develop a highly-sensitive indicator of hmPAC1R activation, we followed a protein
87 engineering approach that we and others recently established[11,14,17]. We used the human

88 PAC1Rnull splice isoform as a protein scaffold (hmPAC1R) and constructed an initial sensor
89 prototype in which we replaced the entire third intracellular loop (ICL3, residues Q336-G342) with
90 a module containing circularly-permuted green fluorescent protein (cpGFP) from dLight1.3b[11]
91 (**Extended Data Fig. 1a**). This initial prototype construct, named PAClight0.1, was expressed on
92 the surface of HEK293T cells, but showed clear intracellular retention and a very weak average
93 fluorescent response to bath application of $PACAP_{1-38}$ ($\Delta F/F_0$ = 43.4%, **Extended Data Fig. 1b**).
94 Using this sensor as template, we conducted a small-scale screen to identify the optimal insertion
95 site by reintroducing amino acids from the original ICL3 of hmPAC1R on both sides of the cpGFP-
96 module. This led us to the identification of a second mutant, in which Q336 was reintroduced
97 before the cpGFP-module, that showed improved average fluorescent response to the ligand
98 ($\Delta F/F_0$ = 343%, **Extended Data Fig. 1c**). To improve membrane expression of the PAClight
99 mutants, we next investigated the effect of point mutations on their C-terminus, via site-directed
100 mutagenesis. Mutation into alanine of residue T468, a reported post-translational modification
101 (PTM) site (www.phosphosite.org) on the C-terminus of the receptor[21], improved the overall
102 surface expression of the sensor in HEK293T cells and further increased the observed average
103 fluorescent response ($\Delta F/F_0$ = 516%, **Extended Data Fig. 1f**). To further improve the fluorescent
104 response of PAClight, we screened a subsequent library of sensor variants with mutations
105 targeted to the second intracellular loop (ICL2). A similar approach was previously shown to boost
106 the fluorescent response of other GPCR-based sensors, for example dLight1.3b or OxLight1[11,17].
107 Our functional screen of a library of ICL2 mutants led to the identification of one variant comprising
108 three point mutations (F259K/F260K/P261K) that displayed a largely improved fluorescent
109 response to $PACAP_{1-38}$ ($\Delta F/F_0$ = 942%, **Extended Data Fig. 1d**). Upon introduction of the C-term
110 T468A mutation on the ICL2 F259K/F260K/P261K background, we obtained an improved version
111 of the sensor, named PAClight1, with excellent surface expression and fluorescent response
112 ($\Delta F/F_0$ = 1037%, **Extended Data Fig. 1g**). Given the high degree of sequence and structural
113 similarity, as well as the broad activation of endogenous VPAC receptors by vasoactive intestinal

114 peptide (VIP) and PACAP[22], we next asked whether the hmPAC1R-based sensor would also
115 respond to VIP. Indeed, application of a high concentration of VIP onto sensor-expressing cells
116 caused a large fluorescent response, corresponding to more than half of the response to $PACAP_{1-}$
117 $_{38}$ ($\Delta F/F_0$ = 654%, **Extended Data Fig. 2c and 2d**). In an effort to eliminate the response to VIP
118 and obtain a PACAP-specific sensor, we screened a small library of sensors containing single-
119 point mutations into alanine that were inspired by simulations on the binding free energy of
120 PACAP and VIP on the PAC1R[23]. Furthermore, at this stage we included the naturally occurring
121 splice mutant PAC1s into the extracellular ligand-binding domain (ECD) of the sensor (this is a
122 short ECD mutant reported to have lower affinity towards VIP[9]), as well as two structure-guided
123 point-mutants. Through this screening, we identified a single mutation (P78A) that abolished the
124 sensor response to VIP while leaving unaltered the response to $PACAP_{1-38}$ (**Extended Data Fig.
125 2c and 2d**). The final sensor construct, named $PAClight1_{P78A}$ (**Figure 1a,b**), includes all the
126 above-mentioned mutations and combines a very large dynamic range with excellent PACAP
127 selectivity and good membrane expression, and was thus selected for further *in vitro*
128 characterization.
129

130 **In vitro characterization of $PAClight1_{P78A}$**

131 The newly developed $PAClight1_{P78A}$ sensor displays an average fluorescent response of
132 1109% $\Delta F/F_0$ in HEK293T cells (n=3, 5 ROIs each) to bath application of 10μM $PACAP_{1-38}$ (**Figure
133 1b-d**). We verified that sensor expression and function is not drastically affected by the cell type
134 in which it is expressed by testing it in primary cultured neurons. Neurons were virally transduced
135 using an adeno-associated virus (AAV) for expressing the $PAClight1_{P78A}$ sensor under control of
136 a human synapsin-1 promoter. 2-3 weeks after transduction we verified excellent expression of
137 the probe on the plasma membrane of the neurons with no appreciable intracellular retention.
138 Under these conditions, the sensor showed a fluorescence response of approximately 730%
139 $\Delta F/F_0$ upon bath application of the $PACAP_{1-38}$ ligand (**Figure 1c,d**).

140 We next set out to determine the sensor's excitation and emission spectra in vitro in HEK29T cells
141 (**Figure 1e**). The excitation maxima in the absence and presence of 10μM $PACAP_{1-38}$ were
142 identified at 504nm and 498nm respectively. The isosbestic point at which the excitation is
143 independent of the absence or presence of $PACAP_{1-38}$ is located at 420nm. The maxima for the
144 emission spectra in the absence of $PACAP_{1-38}$ was identified at 520nm and in the presence of
145 $PACAP_{1-38}$ at 514nm.
146 Our previous work on the development of another class-B1 sensor based on the GLP1 receptor,
147 led us to discover that the kinetics of the sensor's response can be used to infer the occupancy
148 of the ECD by an antagonist peptide[24]. Given that all class-B1 GPCRs share a similar ECD high-
149 affinity ligand binding mechanism, we performed similar experiments to determine whether
150 $PAClight1_{P78A}$ could also be used in a similar manner. To do so, we monitored the sensor's
151 response during application of $PACAP_{1-38}$ alone or in the presence of $PACAP_{6-38}$, an antagonist
152 peptide, in the buffer surrounding the cells. We then determined the activation time constant of
153 the fluorescent response in both conditions. The $PAClight1_{P78A}$ response was strikingly slower
154 (approximately 4-fold) in the presence of the extracellular antagonist, and was in the range of 1
155 second in its absence **(Figure 1f,g)**. Thus, the kinetics of $PACligth1_{P78A}$ response could be used
156 to investigate or screen for factors that influence the ECD-PACAP interaction and potentially the
157 speed of signal transduction through conformational activation of the receptor.
158 To investigate the stability of the fluorescent response to bath application of $PACAP_{1-38}$, a
159 long-term imaging experiment was performed at room temperature with 1 frame (1024x1024
160 pixels, 2x line-averaging) acquired every minute over the time course of 150 min (**Figure 2a**).
161 After bath application of 200nM $PACAP_{1-38}$ (slow diffusion of the peptide with 10x dilution from
162 2μM to 200nM) there was no decrease in signal, nor any internalization observed. After >100
163 frames of acquisition. we applied a saturating bolus of the peptide PAC1R-antagonist Max.d.4.
164 Within 45-50 frames after application of the PAC1R antagonist, the signal intensity steadily
165 decreased and started to plateau slightly above baseline levels. This indicates, that Max.d.4 can

166 outcompete $PACAP_{1-38}$ at $PAClig th1_{P78A}$, albeit not to a full extent under the specified experimental
167 conditions.

168 Next, we screened a range of different peptides at saturating concentrations (10μM) for
169 potential activation of the $PAClight1_{P78A}$ sensor (**Figure 2b**). Mammalian $PACAP_{1-38}$ displayed the
170 strongest potency in $PAClight1_{P78A}$ activation (1052% $\Delta F/F_0$, $t_{(3)}$= 40.31, 95% CI [9.69, 11.35],
171 p<0.001). Because the amino acid sequence of PACAP is rather well conserved throughout
172 phylogeny, we also tested chicken $PACAP_{1-38}$ (chPACAP38), as well as the zebrafish $PACAP2_{1-}$
173 $_{27}$ (zfPACAP2) for potency on the $PAClight1_{P78A}$ sensor. Both of these homologues of the
174 mammalian $PACAP_{1-38}$ activated the $PAClight1_{P78A}$ sensor with strong but slightly reduced
175 potency (chPACAP38: 896% $\Delta F/F_0$, $t_{(4)}$= 11.17, 95% CI [6.73, 11.19], p= 0.0066; zfPACAP2:
176 898% $\Delta F/F_0$, $t_{(3)}$= 11.49, 95% CI [6.46, 11.41], p= 0.024). Furthermore, we also screened the sand
177 fly salivary gland derived peptide Maxadilan, which was previously identified to be a specific ligand
178 of the PAC1R but not to the VPAC1 and VPAC2 receptors[25]. Consistent with the reported activity
179 of Maxadilan on the hmPAC1Rnull receptor, we detected activation of $PAClight1_{P78A}$ by
180 Maxadilan, however, with lower potency than mammalian $PACAP_{1-38}$ (416% $\Delta F/F_0$, $t_{(3)}$= 9.47, 95%
181 CI [2.76, 5.56], p= 0.04). The reduced potency of Maxadilan for $PAClight1_{P78A}$ might be a
182 consequence of the ligand specificity determining point-mutation (P78A) introduced into the
183 extracellular domain of the $PAClight1_{P78A}$ sensor. The drosophila gene *amn* (amnesiac) was
184 previously shown to be homologous to the mammalian gene encoding PACAP (*Adcyap1*) and
185 *amn* drosophila mutants show memory impairments similar to rodent PACAP/PAC1R mutants[26].
186 We therefore also tested whether this insect peptide encoded by *amn* would activate
187 $PAClight1_{P78A}$, but no significant activation above baseline was observed (26% $\Delta F/F_0$, $t_{(2)}$= 3.2,
188 95% CI [-0.09, 0.61], p= 0.69). As shown above (**Extended Data Fig. 2c and 2d**) $PAClight1_{P78A}$
189 was specifically optimized for VIP non-responsive properties. Therefore, the response of
190 $PAClight1_{P78A}$ to VIP in this specificity screen was also not significantly above baseline (57%

191 $\Delta F/F_0$, $t_{(2)}$= 11.09, 95% CI [0.35, 0.79], p= 0.12). Other peptides tested in this screen included
192 other class B1 GPCR ligands (corticotropin-releasing factor (CRF), parathyroid hormone (PTH),
193 and glucagon-like peptide 1 (GLP-1)), as well as some peptidergic class A GPCR ligands
194 (oxytocin (OXY), orexin-A and -B (OXA-OXB), melanin-concentrating hormone (MCH), dynorphin
195 (DYN), enkephalin (ENK), nociception (N-OFQ), neuropeptide FF (NPFF), neuropeptide S (NPS),
196 neurotensin (NT), and neuromedin B (NB)). None of these neuropeptides activated the
197 PAClight1$_{P78A}$ sensor above baseline level (**Figure 2b**). Taken together, these results highlight
198 the broad potential applicability of the PAClight1$_{P78A}$ sensor for use in model systems across the
199 phylogenetic tree, as well as its high selectivity for PACAP ligands over VIP and other peptide
200 GPCR ligands.

201 In order not to induce artificial PACAP signaling and potentially interfere with downstream
202 readouts when using PAClight1$_{P78A}$, it is important to verify that the sensor does not recruit G-
203 proteins and/or β-arrestin. To monitor the capacity of PACLight1$_{P78A}$ to engage these intracellular
204 signaling partners, we performed split NanoLuc complementation assays as in our previous
205 work[17,19], using either PAClight1$_{P78A}$-SmBiT or, as a positive control, PAC1R-SmBiT fusion
206 constructs, together with LgBiT-miniGs (**Extended Data Fig. 3a**), LgBiT-miniGsq (**Extended Data**
207 **Fig. 3b**), or LgBiT-β-arrestin2 (**Extended Data Fig. 3c**). As expected, we observed significant
208 miniGs, miniGsq, and β-arrestin2 recruitment to the wild-type PAC1R upon activation with 1 μM
209 of PACAP$_{1-38}$. Yet, we did not detect recruitment of either miniGs, miniGsq, or β-arrestin2 in
210 PAClight1$_{P78A}$-expressing cells upon stimulation with PACAP$_{1-38}$. These results indicate that
211 expression of PAClight1$_{P78A}$ does not artificially induce PACAP-mediated intracellular signaling
212 and is not likely to interfere with endogenous signaling pathways.

213

214 **Development of non-responsive PAClight1 control sensors**

When employing GPCR-sensors in intact living tissue (e.g., when used in animal models) it is often desirable to make use of an appropriate control sensor, in which ligand-binding is abolished by virtue of one or more point mutations in the GPCR binding pocket. To engineer such control sensors for our PAClight1$_{P78A}$ and PAClight1 sensors, we targeted key residues in the hmPAC1R that interact with residue D3 in PACAP. The carboxylic group of D3 was shown to be crucial for binding affinity and biological activity of PACAP to all three receptor types (i.e. PAC1, VPAC1, and VPAC2)[27,28]. Furthermore, the cryo-EM structure of the hmPAC1R in interaction with PACAP identified residues Y161 and R199 of the hmPAC1R to interact with residue D3 of PACAP[22]. Residue Y161 forms a hydrogen bond with D3, while R199 forms an electrostatic interaction with D3 (**Extended Data Fig. 4a and 4b**). To abolish these interactions, we first mutated R199 into alanine (R199A) on the backbone of PAClight1. This single point mutant showed drastically reduced average fluorescent response (PAClight1: 1075% $\Delta F/F_0$, PAClight1_R199A: 41.9% $\Delta F/F_0$, **Extended Data Fig. 4c**) to 10μM PACAP$_{1-38}$. To further abolish the remaining response, we additionally mutated Y161 into alanine (Y161A) on the previous backbone (i.e. PAClight1_R199A_Y161A) and named the construct "PAClight1-ctrl". This completely reduced the fluorescent response to PACAP$_{1-38}$ to baseline levels (PAClight1-ctrl: 2.87% $\Delta F/F_0$). Next, we cloned these two point mutations into the backbone of PAClight1$_{P78A}$ and observed an equally abolished fluorescent response to PACAP$_{1-38}$ (PAClight1$_{P78A}$: 1034% $\Delta F/F_0$, PAClight1$_{P78A}$-ctrl: 10.44% $\Delta F/F_0$, $t_{(4.03)} = 37.89$, $p < 0.0001$, 95% CI [1098.63, 949.02], two-sided two-sample Welch's *t* test, **Extended Data Fig. 4d**) in transfected HEK293T cells, as well as in virally-transduced rat primary neuron cultures (**Extended Data Fig. 4f)**. No drastic differences in basal brightness were observed between PAClight1$_{P78A}$ and PAClight1$_{P78A}$-ctrl constructs (**Extended Data Fig. 4e)**. In summary, we have developed double point-mutant sensor constructs for both PAClight1$_{P78A}$ and PAClight1 with fully abolished responses to bath application of saturating concentrations of PACAP$_{1-38}$.

240

241 **Comparison between transient and stable expression of the sensor**

242 During the development and validation of PAClight1$_{P78A}$, we noticed higher basal brightness
243 levels of PAClight1$_{P78A}$ compared to other GPCR-based fluorescent sensors. To obtain a
244 quantitative comparison, we decided to produce a stable T-Rex HEK293 cell line for inducible
245 expression of PAClight1 (mutant missing P78A ECD mutation). We then used flow cytometry to
246 record multiple replicates of 100,000 cells, and compared their fluorescence intensity to that of a
247 similarly generated cell line expressing the indicator dLight1.3b, which we previously described[29]
248 (**Figure 2c-d**). Visualization of the fluorescent readouts clearly showed a shift of the density
249 curves towards higher fluorescence for HEK293_PAClight1 cells compared to the
250 HEK293_dLight1.3b. Statistical comparison of the distributions of the two cell lines shows 2.15-
251 fold higher basal brightness of PAClight1 over dLight1.3b ($t_{(4.74)}$= -19.254, p < 0.0001, 95% CI [-
252 1.30, -0.99], two-sided two-sample Welch's *t* test, **Figure 2d**).

253 Among the most important potential advantages of using stable cell lines expressing GPCR
254 sensors for pharmacological assays are the homogeneity of expression, reproducibility, and ease
255 of use. To verify that this is indeed the case, we analyzed PACLight1$_{P78A}$ expressing stable cells
256 and compared them to transfected cells using flow cytometry. While a large proportion of cells
257 from the transfected condition expressed the sensor at very low levels or not at all (i.e., were left
258 shifted in the density plot), we also observed a significant proportion of very bright and strongly
259 expressing cells from within the same condition. In fact, there is higher abundance of very bright
260 and strongly expressing cells in the transfected condition than in the induced stable cell line
261 condition (**Figure 3a**). The combination of the higher abundance of very low expression levels
262 and very high expression levels within the transfected condition leads to a significantly increased
263 variability of observed expression levels compared to the induced stable cell line condition. The
264 median of the standard deviation in the FITC-A channel across the titration series was 62.6%
265 smaller in the stable PAClight1$_{P78A}$ relative to the transfected PAClight1$_{P78A}$ condition (p= 0.0142,

266 **Figure 3b**). The variability of cells transfected with PAClight1 was very comparable and was only
267 8.6% lower than in the PAClight1$_{P78A}$ transfected condition (p= 0.5966, **Figure 3b**). The difference
268 of 8.6% (even though statistically unsignificant) might partially be explained by slightly different
269 performance of PAClight1$_{P78A}$ vs. PAClight1 in dynamic range. *P* values represent the result of
270 Dunnett's test for correction of multiple comparison that was performed after the statistically
271 significant results of an omnibus ANOVA ($F_{(2,30)}$= 4.321, p= 0.0224).

272 With the stable cells and their improved homogeneity of expression levels, we then
273 determined the affinities of PAClight1$_{P78A}$ and PAClight1 towards PACAP$_{1-38}$ and VIP. For each
274 peptide concentration of a titration series 100,000 events were acquired, gated for cell clusters
275 and for singlets. The FITC-A median fluorescence intensity (MFI) of the events in the singlet gate
276 were used for dose-response fitting. A representative PACAP$_{1-38}$ titration series replicate on stable
277 HEK293_PAClight1 cells is shown in **Figure 3c**. The titration dataset reveals a slightly lower
278 affinity of the PAClight1$_{P78A}$ sensor (EC50= 29.91nM) than the PAClight1 sensor (EC50 =
279 22.97nM) towards PACAP$_{1-38}$ (**Figure 3d**). The affinity of the PAClight1 sensor (non-specific
280 mutant) towards VIP (EC50 = 1.238μM) is much lower than its affinity towards PACAP$_{1-38}$ (**Figure**
281 **3d**). This 100-1000x difference is well in accordance with previous reports on the differential
282 affinities of VIP and PACAP$_{1-38}$ on the PAC1R[30,31]. We were not able to detect any response of
283 PAClight1$_{P78A}$ to the addition of VIP up to a concentration of 50μM (linear regression p= 0.079,
284 **Figure 3d**), corroborating the specificity of the PAClight1$_{P78A}$ sensor. Taken together, these data
285 show that the PAClight1$_{P78A}$ and PAClight1 sensors display very high affinity towards PACAP$_{1-38}$,
286 with a slightly lower affinity of PAClight1 compared to PAClight1$_{P78A}$ as the result of the point
287 mutation on the extracellular domain of PAClight1$_{P78A}$.

288

289 **Characterization of PAClight1$_{P78A}$ and PAClight1$_{P78A}$-ctrl in model organism systems**

290 Since PAClight1$_{P78A}$ showed excellent expression and response properties in neuronal cell
291 cultures, we next tested whether the sensor can be established as a tool to test ligand binding in

292 intact neuronal circuits of mammalian model systems. Publicly available RNAseq databases (*in*
293 *situ* hybridization atlas from the Allen Institute: alleninstitute.org) and previous work[32] show strong
294 expression of PACAP (*Adcyap1*) and PACAP receptors (*Adcyap1r1*) in the cerebral cortex and
295 hippocampus of mice and humans, suggesting these structures as interesting candidates for drug
296 targeting. We tested the expression, sensitivity, and specificity of PAClight1$_{P78A}$ in acute mouse
297 brain slices that provide a physiological environment to examine the actions of pharmacological
298 agents within specific brain areas[33].

299 AAVs encoding the PAClight1$_{P78A}$ or PAClight1$_{P78A}$-ctrl sensor under control of a human
300 synapsin-1 promoter were stereotactically injected into the neocortex and hippocampus of adult
301 mice (**Figure 4a**). 4 weeks later, virus expression in the injection site was validated by histology
302 (**Figure 4b**). PAClight1$_{P78A}$ and PAClight1$_{P78A}$-ctrl were efficiently expressed in neuronal cell
303 bodies, axons and dendrites (**Figure 4c, Extended Data Figure 5**).

304 To investigate the sensor response dynamics and its sensitivity, acute brain slices expressing
305 PAClight1$_{P78A}$ or PAClight1$_{P78A}$-ctrl were prepared and PACAP$_{1-38}$ was bath-applied at
306 concentrations ranging from 0nM to 3000nM. We observed a dose-dependent fluorescence
307 increase to PACAP$_{1-38}$ using PAClight1$_{P78A}$, but not PAClight1$_{P78A}$-ctrl (**Figure 4d**). PAClight1$_{P78A}$
308 fluorescence increased by +6.8 and +17.5% $\Delta F/F_0$ when bath-applying 300 and 3000 nM of
309 PACAP$_{1-38}$ respectively (**Figure 4d**). Comparing PAClight1$_{P78A}$ fluorescence with PAClight1$_{P78A}$-
310 ctrl fluorescence revealed a statistically significant difference when bath-applying 3000 nM of
311 PACAP$_{1-38}$ (**Figure 4d**).

312 To assess the specificity of PAClight1$_{P78A}$ to PACAP$_{1-38}$ in comparison to other neuropeptides
313 in acute brain slices, we recorded its response to 3 μM VIP, corticotropin-releasing factor (CRF),
314 and enkephalin (ENK). PAClight1$_{P78A}$ clearly increased its fluorescence in response to 3 μM
315 PACAP$_{1-38}$ (+17.5% peak $\Delta F/F_0$), but not to VIP (-5.5% peak $\Delta F/F_0$), CRF (-4.3% peak $\Delta F/F_0$), or
316 ENK (+1.4% peak $\Delta F/F_0$) (**Figure 4e**).

317 In conclusion, our data show that in acute mouse brain slices, PAClight1$_{P78A}$ detects
318 concentrations of >300nM of PACAP$_{1-38}$ in superfused bath application, while not reacting to other
319 neuropeptides tested.
320
321 **In vivo PACAP detection in behaving mice**
322 To test whether PAClight1$_{P78A}$ can be used to characterize ligand binding and diffusion in vivo
323 in behaving mice, we implanted fiberoptic cannula into the neocortex of mice expressing
324 PAClight1$_{P78A}$ or PAClight1$_{P78A}$-ctrl to image in vivo fluorescence dynamics while microinjecting
325 PACAP$_{1-38}$ through nearby cannula (**Figure 4f**). Microinfusion of PACAP$_{1-38}$ (300 µM, 200 nl) led
326 to peak fluorescence increases of 126% $\Delta F/F_0$ in PAClight1$_{P78A}$-expressing mice. The
327 fluorescence peaked at 28 min and dropped to 88% $\Delta F/F_0$ 1 hour after, when injections were
328 positioned in average approximately 350µm from the recording site. In contrast, PAClight1$_{P78A}$-
329 ctrl-expressing mice showed a fluorescence increase of only 16% $\Delta F/F_0$ (**Figure 4g**).
330 In conclusion, we show that PAClight1$_{P78A}$ can be a useful tool to detect PACAP$_{1-38}$ in vivo
331 with a dynamic range that allows for the detection of drug injections even in the presence of intact
332 endogenous PACAP systems in mice. Moreover, our data suggest that PACAP$_{1-38}$ diffuses
333 efficiently across hundreds of µm, with slow extracellular degradation in neocortical brain areas
334 of mice.
335
336 **Two-photon validation of the sensor in living zebrafish**
337 Zebrafish larvae are an important animal model that has long been recognized for its utility
338 and applicability to drug discovery[34–36]. Moreover, PAC1 signaling has been associated with the
339 adaptive stress response of zebrafish[10,37]. The high degree of amino acid sequence conservation
340 of PACAP across the phylogenetic tree, as well as the *in vitro* response of PAClight1$_{P78A}$ to
341 zebrafish PACAP that we observed, motivated us to also functionally validate our sensor for use
342 in live zebrafish larvae. Based on a publicly available single-cell RNA sequencing (scRNAseq)

343 dataset[38], we identified the olfactory region of 4 day post-fertilization (dpf) old zebrafish larvae to
344 express high levels of *Adcyap1b* in ~75% of cells composing the olfactory region. The presence
345 of *Adcyap1b* expression in the olfactory region was further confirmed with data obtained by
346 Fransworth et al.[39] (**Figure 5a**). To induce expression of PAClight1$_{P78A}$ in the olfactory region, we
347 used the gal4 driver line Tg(GnRH3:gal4ff), which can strongly drive expression (e.g. of
348 GCaMP6s) in the olfactory bulbs (**Figure 5b**). In conjunction with this gal4 driver line, we used
349 Tol2-mediated integration of a UAS-promoted PAClight1$_{P78A}$ construct. At 4dpf we immobilized
350 the larvae with low-melting point agarose and performed two-photon volumetric imaging of the
351 olfactory region for 5 consecutive 3D volumes as baseline. The immobilized zebrafish larvae were
352 then placed onto a micromanipulator platform to inject 50nL of a 1mM PACAP$_{1-38}$ in saline solution
353 or 50 nL of saline only (negative control) into the ventricular space (i.e. ICV injection).
354 Subsequently, the larvae were re-imaged for 15 additional 3D volumes to record potential
355 alterations in the pixel intensity values emitted by the PAClight1$_{P78A}$ sensor (**Figure 5c, 5c'**). We
356 observed a strong increase in PAClight1$_{P78A}$ fluorescence already at ~120 seconds post-ICV
357 injection with $\Delta F/F_0$ levels continuously rising until the end of the post-ICV injection recordings
358 (**Figure 5d, 5d''**). Peak $\Delta F/F_0$ levels and the Area Under the Curve significantly differed between
359 PACAP$_{1-38}$/saline and saline-only injected animals (n_{saline}= 5, $n_{PACAP1-38}$= 5, Kolmogorov-Smirnov
360 test p=0.0079, **Figure 5e, 5e'**). The condition median for peak $\Delta F/F_0$ levels was 70-fold larger in
361 PACAP$_{1-38}$/saline injected animals (145.76% $\Delta F/F_0$) than in saline-only injected animals (2.06%
362 $\Delta F/F_0$) (**Figure 5e**). However, we noticed considerable variability in the extent of the dynamic
363 range displayed by different ROIs within the same and also between different zebrafishes (**Figure**
364 **5d'', 5e'**).
365
366
367
368 **Discussion**

369 In this work we engineered a new family of genetically-encoded fluorescent sensors using the
370 human PAC1R as a GPCR scaffold. Two of the sensors that we developed (PAClight1 and
371 PAClight1$_{P78A}$) exhibit a very high dynamic range (above 1000% $\Delta F/F_0$), excellent expression at
372 the cell surface, high basal brightness, and retain the pharmacological profile and ligand-binding
373 profile of the parent receptor, with the exception of PAClight1$_{P78A}$ whose response to VIP is
374 intentionally abolished via a single point mutation. As part of this sensor family, we also introduced
375 a control sensor harboring the two point mutations R199A and Y161A, in which the response to
376 PACAP$_{1-38}$ is abolished. Given the higher PACAP-selectivity of PAClight1$_{P78A}$, this sensor variant
377 is intended to be employed when there is an experimental need to ensure maximal selectivity of
378 the response for the endogenous ligand PACAP$_{1-38}$ (for example if the sensor is to be used for
379 attempting the detection of endogenous PACAP$_{1-38}$ release). For all other experimental scenarios,
380 PAClight1 can be a better choice, as it retains the original wild-type sequence in its ECD and thus
381 most closely represents the natural ligand-binding profile of the human PAC1 receptor.

382 Importantly, we demonstrate successful expression and functionality of PAClight1$_{P78A}$ and
383 PAClight1$_{P78A}$-ctrl in the mouse brain through stereotactic injection of AAVs encoding the sensor.
384 Additionally, our experiments in zebrafishes, showed intriguing inter- and intraindividual
385 differences in maximal sensor response to ICV injection of the peptide ligand. These could
386 potentially be explained by differences in the expression density of PAClight1$_{P78A}$ within single
387 cells. An intriguing alternative explanation – that receives support from the observation of
388 continuously increasing $\Delta F/F_0$ levels – could be differential diffusion rates of PACAP$_{1-38}$ from the
389 ventricular spaces into the brain parenchyma. Furthermore, there could be a dependence of the
390 extent of the fluorescent response on the spatial distance between PAClight1$_{P78A}$ -expressing
391 cells and the ventricular wall. Under more controlled experimental conditions, PAClight1-
392 expressing zebrafishes (or PAClight1$_{P78A}$, respectively) could therefore potentially be used to
393 investigate and validate diffusion properties of PAC1R ligands in live organisms at a relatively

394 high-throughput or to screen for novel small-molecule or peptide PAC1R agonists and antagonists
395 with improved penetration properties across the ventricular wall.

396 In line with the zebrafish experiments, $PACAP_{1-38}$ microinjections into mouse cortex revealed
397 slow increases in $\Delta F/F_0$ levels even when $PACAP_{1-38}$ was injected only 100s of μm away from the
398 recording site, substantiating the hypothesis of slow diffusion of $PACAP_{1-38}$ through brain tissue.
399 These results show that the new tools introduced in this study can be valuable assets to
400 investigate real-time dynamics of PAC1 receptor activation in response to specific PAC1 receptor
401 agents at a cellular level and in vivo in zebrafish and in the mammalian brain. The in vivo validation
402 of our sensor demonstrates its ability to reveal localized drug or peptide actions and characterize
403 their diffusion dynamics within brain tissue. We therefore suggest that this tool can be employed
404 in applications such as studying the diffusion of novel PAC1-targeting drugs and peptides to
405 provide mechanistic insights into the localization of drug actions in the brain.
406 Notably, in this work we did not demonstrate the use of any of our PAClight sensors for the
407 detection of endogenous PACAP release in tissues or animal models, as our focus was
408 deliberately set on the characterization and validation of the tools for applications to drug
409 screening and/or development across species. Future work could focus on employing these tools
410 to test whether or not they could be suitable for detecting endogenous PACAP/VIP dynamics with
411 high spatiotemporal resolution in tissues or awake behaving animals.
412
413
414
415
416
417 **Methods**
418
419 *Molecular cloning*

420 A synthetic DNA geneblock for the human PAC1R-null receptor sequence (PAC1R) was
421 designed and ordered (Life Technologies) based on the NCBI protein data bank entry

422 “NP_001109.2”. The protein-coding sequence was codon optimized and flanked by HindIII (5’)
423 and NotI (3’) restriction sites for cloning into a pCMV plasmid (Addgene #60360). A hemagglutinin
424 (HA) signal peptide (MKTIIALSYIFCLVFA) was introduced 5’ to the PAC1R coding sequence.
425 Circular Polymerase Extension Cloning (CPEC) was used to replace the intracellular loop 3
426 (Q336-G342) of PAC1R with a cpGFP module from dLight1[11]. For sensor optimization, libraries
427 of sensor variants were created through site-directed mutagenesis. For signaling assays, a linker
428 + SmBit sequence[40] (GNSGSSGGGGSGGGGSSGG + VTGWRLCERILA) was cloned at the
429 3’end of both the PAClight1$_{P78A}$ and the PAC1R sequence. The XhoI cleavage site from within the
430 SmBit linker sequence and the first 4 residues of the SmBit linker (GNSG) were first cloned into
431 the 3’end of the PAClight1$_{P78A}$ and PAC1R sequences using PCR. Subsequently, a restriction
432 digest using XhoI and XbaI restriction enzymes was performed on the SmBit containing plasmid
433 (B2AR-SmBit) as well as on the pCMV_PAClight1$_{P78A}$ and pCMV_PAC1R plasmids. Ligation of
434 the linker+SmBit insert into the linearized backbones was performed after gel extraction and
435 purification of the insert. For generation of stably expressing and inducible Flp-In T-REx 293 cells,
436 the PAClight1$_{P78A}$ and PAClight1 sequences were cloned into the pcDNA5/FRT/TO backbone,
437 respectively, using restriction digest with BamHI and NotI restriction enzymes. Agonist and
438 antagonist plasmids (i.e. PURE_FLAG-TEV-PACAP1-38 and PURE_FLAG-TEV_PACAP6-38
439 respectively) used for validation of the microfluidics platform were obtained by cloning the
440 nucleotide sequences for PACAP$_{1-38}$ and PACAP$_{6-38}$ (obtained as synthetic geneblocks) into the
441 PURE_deGFP backbone using Gibson Assemby. Subsequently, a FLAG-tag (DYKDDDDK) as
442 well as the first 5 residues of the recognition sequence for the TEV protease (ENLYFQ) were
443 cloned upstream of the PACAP sequences into the obtained plasmid. Single colonies were picked
444 and sequence verified. PCR reactions were performed using a Pfu-Ultra II Fusion High Fidelity
445 DNA Polymerase (Agilent), whereas Gibson Assembly was performed using NEBuilder HiFi DNA
446 Assembly Master Mix (New England Biolabs). All sequences were verified using Sanger
447 sequencing (Microsynth).

448

449 *Structural modelling, protein sequence alignment and peptide synthesis*

450 Modelling of protein structure for the PAClight1$_{P78A}$ sensor construct was performed using
451 AlphaFold2[41], using pdb70 as a template mode. The best-scoring prediction was then manually
452 edited using UCSF Chimera (version 1.13.1). Multiple sequence alignment was performed using
453 ClustalOmega[42] and visualized with the Jalview[43] software (version 2). Zebrafish PACAP2$_{1-}$
454 $_{27}$(zfPACAP2), chicken PACAP$_{1-38}$ (chPACAP38), amnesiac, maxadilan (Maxadilan$_{1-61}$), and
455 Max.d.4 peptides were synthesized on an automated fast-flow peptide synthesizer (AFPS) using
456 a previously described protocol[44].

457

458 *Cell culture, imaging and quantification*

459 HEK293T cells (ATCC #CRL-3216) were cultured in DMEM medium (Thermo Fisher)
460 supplemented with 10% FBS (Thermo Fisher) and 1x Antibiotic-Antimycotic (100 units/mL of
461 penicillin, 100µg/mL of streptomycin, and 0.25 µg/mL of Amphotericin B, Thermo Fisher) and
462 incubated at 37°C with 5% CO_2. Cells were transfected at 50-60% confluency in glass-bottomed
463 dishes using the Effectene transfection kit (Qiagen) according to manufacturer instructions, and
464 imaged 24-48h after transfection, as previously described[17]. Primary cultured hippocampal
465 neurons were prepared and transduced as previously described[19]. Before imaging, all cells were
466 rinsed with 1mL of Hank's Balanced Salt Solution (HBSS, Life Technologies) supplemented with
467 Ca^{2+} (2mM) and Mg^{2+} (1mM). Time-lapse imaging was performed at room temperature (22° C) on
468 an inverted Zeiss LSM 800 confocal microscope using either a 40x oil-based or a 20x air objective.
469 Longer-term imaging for determination of internalization/stability as well as reversibility was
470 performed using a 10x air objective, with 1 frame (1024x1024 pixels) acquired every minute (2x
471 pixel averaging). Imaging was performed using a 488nm laser as excitation light source for
472 PAClight1 sensors. During imaging, ligands were added in bolus on the cells using a micropipette
473 to reach the final specified concentrations of ligands on the cells. For quantification of recordings

474 in single dishes, regions of interest (ROI) were selected manually using pixel-intensity based
475 thresholding in Fiji to isolate the cell membrane. Sensor response ($\Delta F/F_0$) was calculated as the
476 following: (F(t)-F_base)/F_base with F(t) being the ROI fluorescence value at each time point (t),
477 and F_base being the mean fluorescence of the 10 time points prior to ligand addition.
478
479 *Stable cell line generation and maintenance*
480 The stable cell line for tetracycline-inducible expression of PAClight1$_{P78A}$ was generated
481 following previously described procedures[29]. Flp-In T-REx 293 cells were grown in DMEM
482 supplemented with 10% (v/v) fetal bovine serum (FBS; Invitrogen), 100µg/mL zeocin
483 (ThermoFisher Scientific), and 15µg/mL blasticidin (ThermoFisher Scientific). To obtain a cell line
484 with stably-integrated PAClight1$_{P78A}$ or PAClight1 expression cassettes, cells were grown in T150
485 flasks (Corning) until 70% confluency, were then transfected with 0.6µg of pcDNA5/FRT/TO-
486 PAClight1$_{P78A}$ DNA vector and 5.4µg pOG44 vector using Effectene transfection kit (Qiagen). Two
487 days after transfection, cells were split and the medium was changed to DMEM supplemented
488 with 10% (v/v) FBS, 200µg/mL Hygromycin B (Sigma), and 15µg/mL blasticidin. The medium was
489 then replaced twice a week until individual colonies were visible. An individual colony was
490 manually selected and expanded for subsequent experiments. Induction of PAClight1$_{P78A}$ or
491 PAClight1 expression was obtained by adding 1µg/mL doxycycline (Sigma) to the cell medium 1-
492 2 days prior to experimentation.
493
494 *Spectral characterization of the sensors*
495 One-photon spectral characterization of the PAClight1$_{P78A}$ sensor was performed using
496 PAClight1$_{P78A}$-transfected HEK293T cells before and after addition of PACAP$_{1-38}$ (10µM). One-
497 photon fluorescence excitation (λ_{em} = 560nm) and emission (λ_{exc} = 470nm) spectra were
498 determined on a Tecan M200 Pro plate reader at 37°C. 24 hours after cell transfection in 6-well
499 format (linear PEI), ~1 million cells were dissociated with addition of TrypLE Express

500 (ThermoFisher) and thoroughly washed with PBS. Next, cells were resuspended in 300µl of PBS
501 and aliquoted into two individual wells of a 96-well microplate with or without $PACAP_{1-38}$ (10µM),
502 together with two wells containing the same amount of non-transfected cells to account for
503 autofluorescence and a single well containing PBS for subtraction of the Raman bands of the
504 solvent.
505
506 *Flow cytometry*
507 HEK293T cells and stable HEK293_PAClight1$_{P78A}$/PAClight1 cells were seeded into T175
508 flasks and grown to 50-60% confluency under culture conditions described above. HEK293T cells
509 were then transfected with 20µg of pCMV_PAClight1$_{P78A}$ or pCMV_PAClight1 using linear PEI
510 (Sigma-Aldrich; #764965) and a PEI-to-plasmid ratio of 3:1. Stable
511 HEK293_PAClight1$_{P78A}$/PAClight1 cells were induced with 1µg/mL doxycycline (Sigma) at 50-
512 60% confluency. Two days after transfection or induction, cells were washed in 1x PBS before
513 detachment with TrypLE Express (ThermoFisher) and subsequent centrifugation at 150xG for 3
514 minutes. Palleted cells were then resuspended in ice-cold FACS buffer containing 1xPBS, 1mM
515 EDTA, 25mM HEPES (pH 7.0), 1% fetal bovine serum and diluted to 4-4.8x10^6 cells/mL. A dilution
516 series of $PACAP_{1-8}$ and VIP was prepared in FACS buffer. 125µL of peptide solution was pipetted
517 into a 96-well format and another 125ul of cell suspension was added to each well. The 96-well
518 U-bottom plate was then loaded into a BD FACS Canto II cytometer equipped with a high-
519 throughput sampler for 96-well format sampling. Voltage for the photomultiplier tubes was set to
520 200V for the forward scatter detector, to 400V for the side scatter detector, and to 350V for the
521 FITC channel fluorescence detector. Excitation was performed at 488nm, while emission was
522 directed through a 502LP mirror and a 530/30 band pass filter. Sampling from 96-well format wells
523 was performed with an initial mixing step (3x 100µl mixes at 150µL/s) followed by sample
524 acquisition of 200µL at a flow rate of 1-3µL/s. Sampling was performed until 100K events were
525 recorded per well. After sample acquisition of each well, a 800µL wash step of the sampling line

526 was performed. Sample acquisition within a dilution series replicate was performed from low-to-
527 high concentrations to minimize potential peptide carry-over into the neighboring wells.
528 Furthermore, a minimum of six wells without PACAP or VIP present were sampled between each
529 replicate of the same construct. Raw data was exported in FCS3.1 format and further processed
530 for analysis within R. The following R packages were used for the analysis and visualization of
531 the flow cytometry experiments: flowCore, flowAI, ggcyto, dplyr, tidyr, forcats, purrr, stringr,
532 openCyto, openxlsx, svglite, ggprism, ggnewscale, and glue. After import of the raw datasets, a
533 rectangular gate ("Cells") was defined on a FSC-A vs. SSC-A scatter plot with the limits being set
534 to 25K-infinity and 15K-infinity, respectively. Next, a "Singlet" gate within the parent gate "Cells"
535 was created automatically using the openCyto::singletGate function based on the FSC-A vs. FSC-
536 H scatter plot. Median fluorescence intensities (MFI) of the FITC-A channel for all recorded events
537 within the "Singlet" gate were calculated for each well. The MFI values were then normalized
538 ("NormFITC_A") within each titration replicate to the average of the 0nM peptide condition. Dose-
539 response-curves and EC_{50} values were obtained by first grouping datasets by construct and
540 peptide conditions. For each group, a non-linear least squares model was fit using the following
541 formula:

542 $$NormFITC_A \sim \min + ((\max - \min) / (1 + \exp(hill_coefficient * (EC50 - Conc_M))))$$

543 For the VIP titration on the non-responsive sensor variant, a linear regression model was fit using
544 the following formula:

545 $$NormFITC_A \sim Conc_M$$

546

547 *NanoLuciferase complementation assays*

548 HEK293 cells were seeded in 6-well plates and transfected with 0.25µg LgBiT-miniG (miniGs
549 or miniGsq[45]) or LgBiT-β-arrestin2[40] and 0.25µg SmBiT-tagged receptor plasmids using 3µL
550 Lipofectamine 2000 (Thermo Fisher). 24 hours after transfection, cells were plated onto black
551 clear-bottomed 96-well plates at 50,000 to 100,000 cells/well or 384-well plates at 20,000 to

552 30,000 cells/well in DMEM without phenol red, supplemented with 30mM HEPES (pH 7.4) and
553 Nano-Glo Live Cell Reagent (Promega), and incubated for 45 min at 37°C. Luminescence signal
554 was measured simultaneously across the plate using the FDSS/µCELL plate reader
555 (Hamamatsu). Baseline luminescence (before agonist addition) was acquired for 3min. Vehicle
556 (buffer) or agonist ($PACAP_{1-38}$, 1µM) were added simultaneously into wells by an integrated
557 dispensing unit. Luminescence was recorded every 1 – 2 s for 8 min post agonist addition.
558 Agonist-treated wells were initially normalized to vehicle wells, luminescence intensity was then
559 normalized to the baseline prior to ligand addition.
560

561 *Generation and imaging of transgenic fishes*

562 The $PAClight1_{P78A}$ sequence was cloned into a Tol2 transposase-based plasmid[46] with a UAS
563 promoter. The plasmid (75ng/ul) was injected into *Tg(GnRH3:gal4ff)*[47] embryos at the single-cell
564 stage along with transposase mRNA (25 ng/ul). Embryos were sorted at 3 days post fertilization
565 using the red heart marker (cmlc:mCherry) in the *UAS:PAClight1*$_{P78A}$ construct. Positive zebrafish
566 larvae were immobilized using alpha-bungarotoxin (1mg/ml for 30 s) and mounted ventrally
567 (ventral side down) on to a custom molded 3 cm plate using 0.8% low-melt agarose (Sigma-
568 Aldrich). Plates were perfused with E3 media (5mM NaCl, 0.17mM KCl, 0.33mM $CaCl_2$, 0.33mM
569 $MgSO_4$ in H_2O) prior to imaging. Larvae were imaged under the Leica TCS SP8 Multi-Photon
570 Microscope with a 25X/0.95NA water immersion objective. Volumetric images across time were
571 obtained after irradiation at 890 nm at 400 Hz/frame with 2x averaging. Larvae were imaged for
572 five volumes in the naïve state followed by intracerebroventricular injections (ICV) of 1mM
573 PACAP-38 (Sigma-Aldrich) in saline solution (0.6% NaCl, 0.02% Na_2CO_3) and only saline for
574 controls. Larvae were then re-imaged approximately 120 seconds after ICV injection using the
575 same imaging parameters for 15 volumes. Basal and post-injection images were concatenated
576 and registered using descriptor-based series registration on ImageJ/Fiji
577 (https://github.com/fiji/Descriptor_based_registration.git). Raw fluorescence traces were

578 extracted from these images from manually drawn ROIs around cells. Statistical analysis and
579 plotting of graphs were performed in MATLAB and R. Baseline fluorescence, F_0, was computed
580 using basal fluorescence intensities, which were then used to calculate $\Delta F/F_0$. The Kolgomorov-
581 Smirnov t-test was performed where applicable. Single cell transcriptomic data[39] from 4dpf
582 zebrafish larvae was plotted as a function of UMAPs in the UCSC cell browser. High expression
583 of adcyap1b (PACAP) was visualized in Cluster 94 (https://cells.ucsc.edu/?ds=zebrafish-
584 dev&gene=ENSDARG00000027740). Tg(GnRH3:gal4ff) transgenic line was used to express the
585 PAClight1$_{P78A}$ in the olfactory bulb (OB). To confirm that GnRH3 cells were indeed present in the
586 OB at 4dpf, a UAS:GCaMP6s construct was expressed in the Tg(GnRH3:gal4ff) line.
587
588 *Virus production*
589 The biosensor AAV constructs were cloned in the Patriarchi laboratory, while the opsin AAV
590 construct was constructed by the Viral Vector Facility of the University of Zürich (VVF). All viral
591 vectors were produced by the VVF. The viral titers of the viruses used in this study were:
592 AAV9.hSyn.PAClight1$_{P78A}$, 0.75-1.5 x 10^{13} GC/mL, AAV9.hSyn.PAClight1$_{P78A}$-ctrl, 1.6 x 10^{13}
593 GC/mL
594
595 *Animals*
596 Rat embryos (E17) obtained from timed-pregnant Wistar rats (Envigo) were used for
597 preparing primary hippocampal neuronal cultures. Wild-type C57BL/6JRj mice (Janvier, 6-10
598 weeks old) of both sexes were used in this study. Mice were kept in standard enriched cages with
599 *ad libitum* access to chow and water on either normal or reversed 12-h/12-h light/dark cycle. Mice
600 were housed in cages of 2-5 animals.
601 All procedures in mice were performed in accordance with the guidelines of Medical
602 University of Vienna and under approved licenses by the Austrian Ministry of Science.

603 Zebrafish were maintained and bred by standard protocols and according to FELASA guide-
604 lines. All experiments using zebrafish were approved by the Weizmann Institute's Institutional
605 Animal Care and Use Committee (Application number 06340722-1).
606
607 *Stereotactic surgeries*
608 For ex vivo slice imaging and validation of mouse brain expression, 6 to 10-week-old male
609 and female C57BL/6JRj mice (Janvier) were anesthetized with 5% isoflurane and maintained
610 under stable anesthesia during the surgery (1.3-2% isoflurane). Lidocaine (3.5mg/kg; Gebro
611 Pharma, #100562 1404) and Carprofen (4mg/kg; Zoetis, #256684) were administered
612 subcutaneously for local anesthesia and general analgesia. A small craniotomy was made
613 bilaterally, targeting the temporal neocortex (Injection site at -4.1 mm posterior to bregma, as
614 lateral as possible and 1.2 mm ventral to the pial surface). A glass micropipette was used for virus
615 delivery and inserted slowly into the brain. Before and after virus delivery, the micropipette was
616 kept in place for a waiting time of 8 min. 200nL of AAV9.hSyn.PAClight1$_{P78A}$ or
617 AAV9.hSyn.PAClight1$_{P78A}$-ctrl were injected, with an injection rate of 40nL/min using a
618 microsyringe pump (KD Scientific; #788110). The pipette was withdrawn slowly and the skin of
619 the skull was sutured. The mice were allowed to recover for 4 weeks before being used for the
620 experiments, with Carprofen (4 mg/kg) being administered on the two consecutive days after the
621 surgery.
622
623 *Slice imaging*
624 The mice were deeply anesthetized with isoflurane before being sacrificed by a transcardial
625 perfusion with 30mL cooled sucrose solution (212mM sucrose, 3mM KCl, 1.25mM Na2H2PO4,
626 26mM NaHCO3, 1mM MgCl2, 0.2mM CaCl2, 10mM glucose) oxygenated with carbogen gas. The
627 mice were decapitated and the brain was dissected out. 300μM coronal slices were prepared
628 using a Leica VT1200 vibratome in cold oxygenated sucrose solution (0.12 mm/s, 0.8 mm

629 amplitude). The slices were incubated in oxygenated Ringer's solution (125mM NaCl, 25mM
630 NaHCO3, 1.25mM NaH2PO4, 2.5mM KCl, 2mM CaCl2, 1mM MgCl2, 25mM glucose) at 37°C for
631 10min and afterwards kept at room temperature. The slices were imaged using an Olympus
632 BX51WI microscope with an ORCA-Fusion Digital CMOS camera (Hamamatsu, #C14440-20UP)
633 and a 10x objective (UMPLFLN10XW objective, Olympus). An EGFP filterset was used to control
634 emission and excitation spectra (470/40, 525/50; AFH #F46-002). Micromanager software [48] was
635 used to synchronize the excitation LED with the camera shutter. Videos were taken at 4 Hz
636 framerate using 100 ms exposure time per frame. Cortical areas with clearly visible baseline
637 fluorescence were selected for imaging. Baseline recordings of 10-20 min were performed prior
638 to data acquisition to allow the slices to accustom to the conditions. Bath temperature was set to
639 ~31°C. The experimental recording was 20 min long, with the respective peptide being infused
640 from minute 3-5. The following peptides were used: $PACAP_{1-38}$ (30-3000nM; Phoenix
641 Pharmaceuticals; #052-05), VIP (3000nM; Phoenix Pharmaceuticals; #064-16), CRF (3000nM;
642 Phoenix Pharmaceuticals; #019-06), and Met-Enkephalin (3000nM; Phoenix Pharmaceuticals;
643 #024-35). Of note, since our preliminary data suggested a decrease in $PAClight1_{P78A}$ fluorescence
644 in response to 3 μM CRF, we enriched the Ringer's solution with synaptic transmission and
645 neuronal activity blockers (NBQX, CPP, CGP 55845, Gabazine, and TTX) to prevent recruitment
646 of neuronal circuits that could lead to endogenous $PACAP_{1-38}$ release (Tocris, biotechne; #Tocris
647 1262/50, #Tocris 0373/50, # Tocris0247/50, #Tocris 1248/50, #Tocris 1069/1).

648 Data analysis was performed using a custom-written Matlab script. Movement correction as
649 well as bleaching correction was performed. The average fluorescence across the whole imaging
650 window was normalized to the baseline fluorescence measured during the first 3 min of the
651 recording prior to peptide infusion to calculate $\Delta F/F_0$: (F(t)-F_base)/F_base with F(t) being the
652 fluorescence value at each time point (t), and F_0_base being the mean fluorescence of the first
653 3min. 6 slices from at least 3 different mice were averaged for calculating the dose-response

654 curve. For PAClight1$_{P78A}$ responses to VIP, CRF and ENK, 3 slices from 3 different mice were
655 averaged.
656
657 *In vivo photometric imaging and microinfusion*
658 Craniotomies were made as described for stereotactic injections. Tapered fiberoptic cannula
659 implants (MFC_200/230-0.37_2mm_MF1.25_A45) with low autofluorescence epoxy were
660 implanted into the right neocortex at 0.9mm depth with the angled (uncoated) side of the fiber tip
661 facing towards the left. The implant was stabilized with cyanoacrylate glue.
662 Cannula were surgically implanted to locally infuse PACAP$_{1-38}$ into the cortex. Stainless steel
663 guide cannulae (26 gauge; C315GA/SPC, InVivo One, Roanoke, VA, USA) were positioned in
664 cortical L1, such that the tip of the internal cannula terminated 400µm medial to an the fiberoptic
665 cannula. The implant was secured with cyanoacrylate glue. Dummy cannulae that did not extend
666 beyond the guide cannulae (C315DC/SPC, InVivo One) were inserted to prevent clogging.
667 Mice were handled for 7 days prior to drug infusions.
668 For photometric recordings, a 200µm diameter and 0.37 NA patchcord (MFP_200/220/900-
669 0.37_5m_FCM-MF1.25, low autofluorescence epoxy, Dorics) was used to connect the implanted
670 fiberoptic cannulae to a Dorics filter cube for blue (465-480nm) excitation light. Emission light was
671 detected by built-in photodetectors (500-540nm). Signals from the photodetectors were amplified
672 with Dorics built-in amplifiers and acquired using a Labjack (T7). LJM Library (2018 release) was
673 used to allow communication between MATLAB and Labjack. The voltage output from the LED
674 drivers was amplitude modulated at 171 Hz (sine wave) as described previously [49] Amplitude
675 modulation was programmed in MATLAB. 470 nm LEDs (M470F3, Thorlabs; LED driver LEDD1B,
676 Thorlabs) were used. Light power at the patchcord tip was set to an average of 45µW.
677 Fluorescence was calculated with custom-written MATLAB scripts based on a previous
678 publication (Owen and Kreitzer, 2019). Photometry data were sampled at 2052 Hz.

679 For drug infusions, dummy cannulae were replaced by internal cannulae (33 gauge;
680 C315LI/SPC, InVivo One) that extended 1 mm beyond the guide cannulae and were connected
681 to a microinfusion pump. After a recovery time of 5-10 min, $PACAP_{1-38}$ (200nl; 300µM diluted in
682 normal Ringer solution, NRR) was infused at 100 nl/min (NRR in mM: 135 NaCl, 5.4 KCl, 5
683 HEPES, 1.8 CaCl2, pH 7.2 adjusted with KOH, sterile-filtered with 0.2µm pore size).
684
685 *Histology*
686 To verify expression of the sensor in the mouse cortex and hippocampus, virus injections
687 were performed with stereotactic surgeries as described above. The virus was allowed to express
688 for four weeks, before the mice were transcardially perfused with PBS and 4% paraformaldehyde,
689 before the brain was dissected and processed into 50µm coronal slices using a Leica VT1000S
690 vibratome. Slices were immunostained with chicken anti-GFP antibodies (Abcam Cat# ab13970,
691 RRID:AB_300798; 1:500 diluted). In brief, slices were permeabilized and blocked for 1 h with PBS
692 containing 5% NGS and 0.2% Triton X-100, followed by a 24 h antibody incubation at 4°C in PBS
693 containing 5% NGS and 0.2% Triton X-100. Sections were washed in PBS and then incubated
694 for 1 h in 1:500 diluted goat anti-chicken IgG (H+L) cross-adsorbed secondary antibody (Alexa
695 fluor 488; Fisher Scientific A11039). The mounted slices were imaged using a Leica SP8 X
696 confocal microscope equipped with a 63x 1.3 NA glycerol immersion objective.
697
698 *Statistical analysis*
699 For pairwise analysis of sensor variants, the statistical significance of their responses was
700 determined on a case-by-case basis using a two-tailed unpaired Student's t-test with Welch's
701 correction. Analysis of variance (ANOVA) testing was followed by pairwise comparison with
702 correction for multiple comparison with either Dunnett's correction or Hochberg correction. For
703 data not meeting assumptions of normality or homoscedasticity, Mann-Whitney-U tests followed
704 by Bonferroni corrections were applied. All p-values are indicated either in the results section or

705 in the figure legends. Data of sensor screening and validation experiments is displayed as mean
706 +/- 1 standard deviation. No statistical methods were used to predetermine sample size in cultured
707 cells. Power calculations were performed to determine sample size for experiments using mice.
708
709
710

AUTHOR CONTRIBUTIONS

TP led the study. TP and RBC conceived the development of the PAClight sensors. RBC performed all *in vitro* molecular cloning and screening that led to the development of PAClight sensors and characterized the optical and pharmacological properties of the sensor under the supervision of TP. AG measured and analyzed sensor kinetics under the supervision of TP. EW and PH synthesized peptides under supervision of NH. KA performed intracellular signaling assays under the supervision of MS. MAB prepared cultured neurons under the supervision of DB. SN and SM performed and analyzed imaging experiments in acute brain slices and in vivo photometry recordings and microinfusions under the supervision of SM. PR performed the in vivo experiments using zebrafish under the supervision of GL. TP and RBC wrote the manuscript with contributions from all authors.

DATA AVAILABILITY

The DNA and protein sequence of the sensor developed herein have been deposited on NCBI (accession number OQ366523) and are available in Supplementary Data S1. Viral DNA plasmids have been deposited both on ADDGENE and on the UZH Viral Vector Facility (https://vvf.ethz.ch/). Viral vectors can either be obtained from the Patriarchi laboratory, the UZH Viral Vector Facility, or Addgene. Data presented in this manuscript are available from the authors upon reasonable request.

CODE AVAILABILITY

Custom written code can be made available upon request.

ACKNOWLEDGEMENTS

The results are part of a project that has received funding from the European Research Council (ERC) under the European Union's Horizon 2020 research and innovation program

(Grant agreement No. 891959) (TP). We also acknowledge funding from the Swiss National Science Foundation (Grant No. 310030_196455 and 310030L_212508), Olga Mayenfisch Foundation, and Hartmann Müller Foundation for Medical Research (TP). PR is supported by a research grant for student's fellowship from the Benoziyo Endowment Fund for the Advancement of Science and by the Weizmann–CNRS Collaboration Program. GL lab is supported by the Israel Science Foundation (#349/21); Israel Ministry of Science and Technology (#3-16548) and Hedda, Alberto, and David Milman Baron Center for Research on the Development of Neural Networks. MS and KA are supported by a Swiss National Science Foundation Eccellenza Professorial Fellowship to M.S. (PCEFP3_181282). SM and SN have been funded by the Vienna Science and Technology Fund (WWTF) and the City of Vienna through project VRG21-015. We would like to thank Prof. Marco Celio for generously contributing financial support during the project.

COMPETING FINANCIAL INTERESTS

TP is a co-inventor on a patent application related to the technology described in this article. All other authors have nothing to disclose.

Figure 1

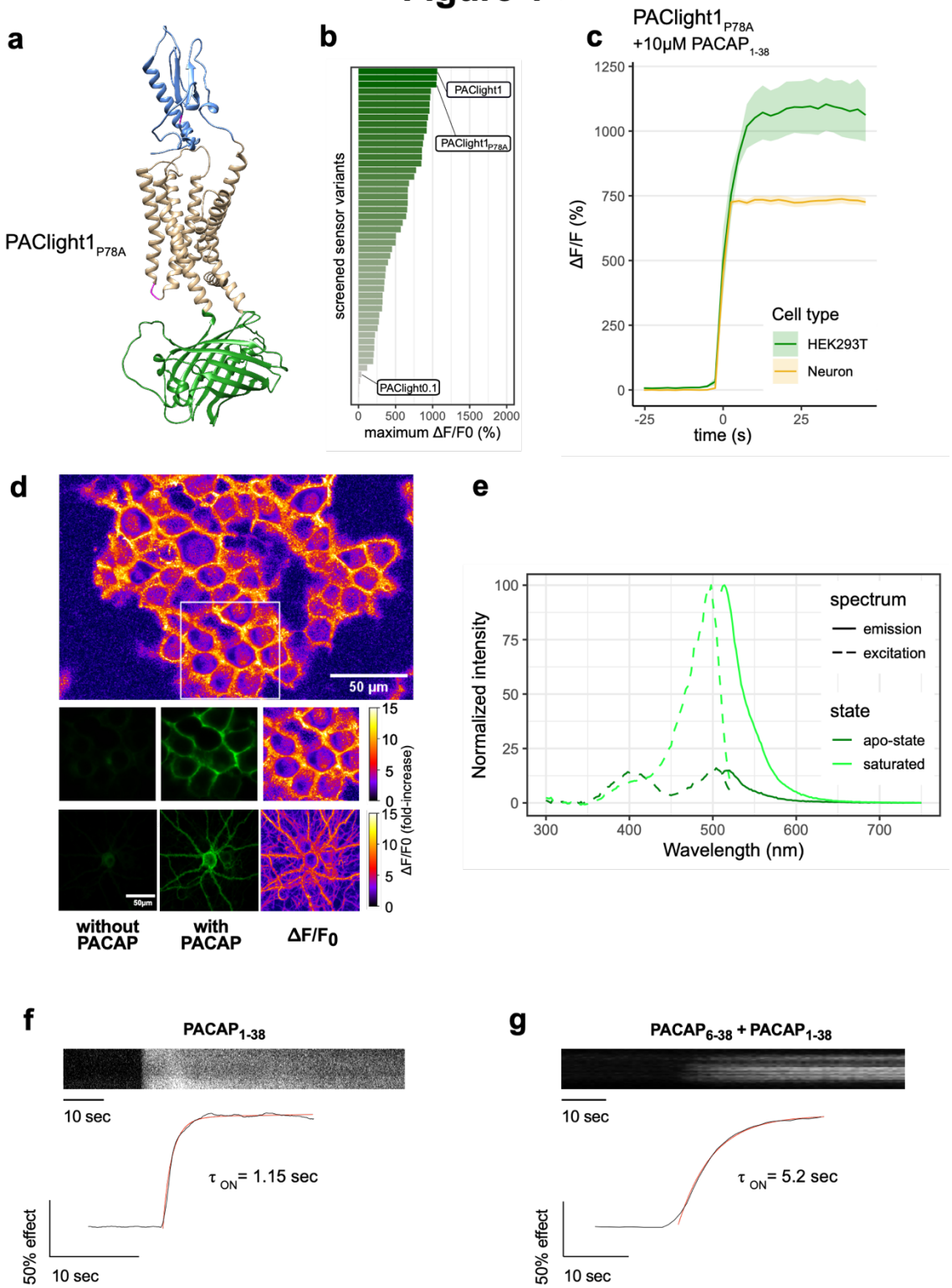
a
PAClight1P78A
b
screened sensor variants
PAClight1
PAClight1P78A
PAClight0.1
0 500 1000 1500 2000
maximum ΔF/F0 (%)
c
PAClight1P78A
+10μM PACAP1-38
1250
1000
750
500
250
0
ΔF/F (%)
-25 0 25
time (s)
Cell type
HEK293T
Neuron
d
50 μm
15
10
5
0
ΔF/F0 (fold-increase)
without PACAP
with PACAP
ΔF/F0
e
Normalized intensity
100
75
50
25
0
300 400 500 600 700
Wavelength (nm)
spectrum
emission
excitation
state
apo-state
saturated
f
PACAP1-38
10 sec
τ ON= 1.15 sec
50% effect
10 sec
g
PACAP6-38 + PACAP1-38
10 sec
τ ON= 5.2 sec
50% effect
10 sec

Figure 1 | Design and in vitro optical properties of PAClight1$_{P78A}$

a) Protein structure of PAClight1$_{P78A}$ as predicted by AlphaFold2[50]. The transmembrane and intracellular domain of the PAC1Rnull backbone is depicted in beige. The extracellular domain, which is crucial for ligand specificity and affinity, is colored in blue. The cpGFP module replacing the 3rd intracellular loop is colored in green. Point-mutations inserted in the 2nd intracellular loop as well as on the extracellular domain are depicted in magenta. **b)** Bar chart depicting the maximum dynamic range obtained for all tested mutants with acceptable expression on the plasma membrane. Bars are ordered by dynamic range and color coded by the average of the maximum dynamic range recorded. The bars representing the prototype variant PAClight_V0.1, PAClight1$_{P78A}$ and PAClight1 are indicated. **c)** Representative line plots depicting the maximum activation (mean +/- SEM) of PAClight1$_{P78A}$ expressed in HEK293T cells and rat primary neurons. Upon bath application of 10µM PACAP$_{1-38,}$ PAClight1$_{P78A}$ reaches a $\Delta F/F_0$ of 1055% in HEK293T cells (n=1, 5 ROIs) and a $\Delta F/F_0$ of 729% in rat primary neurons (n=1, 8 ROIs). Confocal image acquisition was performed at a frame rate of 1 frame/2.53s (~0.4Hz). **d)** Representative examples of the expression of PAClight1$_{P78A}$ in HEK293T cells (low magnification overview and middle row of images) and rat primary neurons (bottom row) with pixel-wise quantification and depiction of the dynamic range in $\Delta F/F_0$ upon bath application of 10µM PACAP$_{1-38}$. Top: Overview micrograph of HEK293T cells color coded in pixel-wise $\Delta F/F_0$. The white square represents the ROI represented below in the middle row of images. Middle: Selected ROI before (left) and after (middle and right) peptide application. Bottom: Rat primary neuron expressing PAClight1$_{P78A}$ before (left) and after (middle and right) peptide application. The color bars represent the look-up table used for visualization of the pixel-wise $\Delta F/F_0$. **e)** One-photon excitation (dashed lines) and emission (solid lines) spectra of PAClight1$_{P78A}$ in the absence (apo-state, dark green) and the presence (saturated state, light green) of 10µM PACAP$_{1-38}$. The excitation maximum of the saturated state is at 498nm. The isosbestic point is at 420nm. Emission maximum in of the saturated state is at 514nm. **f**) Activation kinetics of PAClight1$_{P78A}$ upon application of PACAP$_{1-38}$ (10 µM) measured via timelapse imaging. A representative kymograph of sensor fluorescence on the surface of a HEK293 cell is shown on top. The normalized fluorescence response trace is shown at bottom along with the calculated one-phase association curve fit and activation time constant. The trace shown is the average of 3 independent experiments. **g**) Same as **f)** but in the presence of PACAP$_{6-38}$ (10 µM) in the bath.

Figure 2

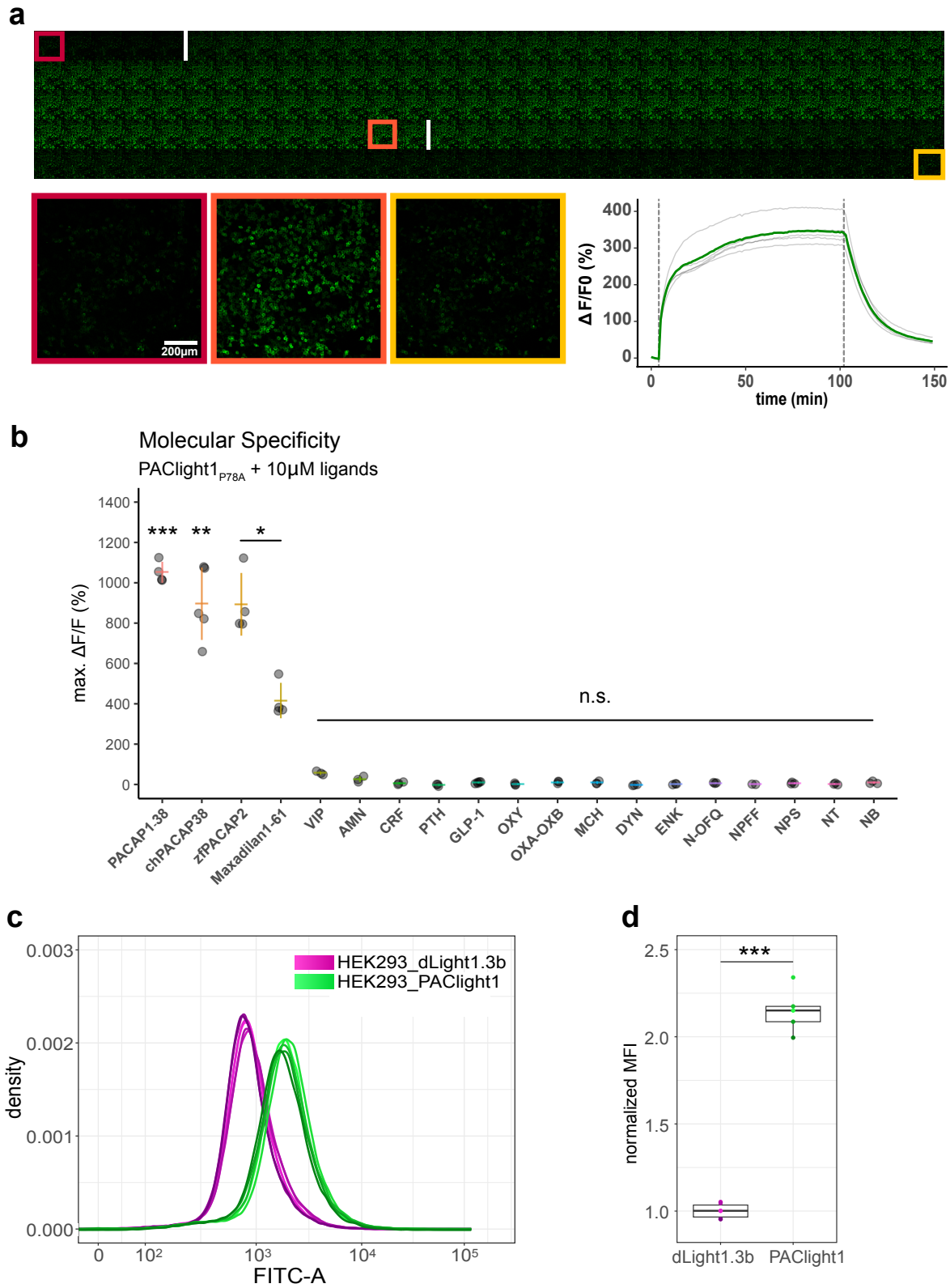
a
200µm
ΔF/F0 (%)
time (min)
b
Molecular Specificity
PAClight1P78A + 10µM ligands
max. ΔF/F (%)
***
**
*
n.s.
PACAP1-38
chPACAP38
zfPACAP2
Maxadilan1-61
VIP
AMN
CRF
PTH
GLP-1
OXY
OXA-OXB
MCH
DYN
ENK
N-OFQ
NPFF
NPS
NT
NB
c
HEK293_dLight1.3b
HEK293_PAClight1
density
FITC-A
d
normalized MFI
dLight1.3b
PAClight1

789

Figure 2 | Pharmacological characterization of PAClight1$_{P78A}$

a) PAClight1$_{P78A}$ fluorescent response to 200 nM PACAP$_{1-38}$ bath application over extended periods at room temperature. No internalization of the sensor expressed on the plasma membrane is observed throughout the full time course of >90 minutes. The fluorescent response of PAClight1$_{P78A}$ to PACAP$_{1-38}$ can be reversed with competitive binding of the peptidergic PAC1R antagonist Max.d.4 (a Maxadilan derivative). Please note that the seemingly slow activation rate of PAClight1$_{P78A}$ in this experiment is due to the experimental setup (see methods section) and slow diffusion of PACAP$_{1-38}$ throughout the well. Top: Downscaled gallery view of the acquired time series (total of 150 frames; 1 frame/minute) from top-left to bottom-right. Application time points of PACAP$_{1-38}$ (after frame Nr. 5) and Max.d.4 (after frame Nr. 103) are depicted as white vertical lines between the frames. The red, orange, and yellow rectangles indicate the frames used for representative higher magnification inserts shown below (bottom left). Bottom right: Line plot depicting the time course of the PAClight1$_{P78A}$ response across 5 rectangular ROIs distributed across the whole field of view. **b)** PAClight1$_{P78A}$ is highly specific to PACAP and does not respond to VIP. PAClight1$_{P78A}$ can be activated by PACAP homologues found in the chicken (gallus gallus, chPACAP38) as well as in the zebrafish (danio rerio, zfPACAP2). PAClight1$_{P78A}$ is further partially activated by the PAC1R specific ligand Maxadilan$_{1-61}$, which is expressed endogenously in the sand fly (Lutzomyia longipalpis) salivary gland. None of the other tested class A and B1 GPCR ligands was found to activate PAClight1$_{P78A}$. Abbreviations: AMN amnesiac, CRF corticotropin-releasing factor, PTH parathyroid hormone, GLP-1 glucagon-like peptide, OXY oxytocin, OXA-OXB orexin-A and -B, MCH melanin-concentrating hormone, DYN dynorphin, ENK enkephalin, N-OFQ nociception, NPFF neuropeptide FF, NPS neuropeptide S, NT neurotensin, NB neuromedin B. Single data points represent one replicate average obtained from 5 ROIs per replicate. The extent of the colored vertical bar represents 1 standard deviation. The y-axis location of the colored horizontal bar indicates the average across all replicates. Number of replicates per ligand: n=5 for chPACAP38 and GLP-1; n=4 for PACAP$_{1-38}$, zfPACAP2, and Maxadilan$_{1-61}$; n=3 for VIP, AMN, CRF, PTH, OXY, OXA-OXB, MCH, DYN, ENK, N-OFQ, NPS, NT, and NB; n=2 for NPFF. Asterisks represent statistical significance of Hochberg-corrected *p* values of multiple one-sample *t* tests. **c)** PAClight1 has significantly brighter baseline fluorescence than the dopamine sensor dLight1.3b. The peak of the dLight1.3b FITC-A density curve coincides with the start of the uphill slope of the PAClight1 FITC-A density curve. Note the bi-exponential scaling of the x-axis. n=6 for dLight1.3b, n=5 for PAClight1. **d)** Quantification of the average of the median fluorescence intensity (MFI) across all replicates and normalization to the group MFI of dLight1.3b show a 2.15-fold increased basal brightness of PAClight1 over dLight1.3b ($t_{(4.74)}$= -19.254, $p < 0.0001$, 95% CI [-1.30, -0.99], two-sided two-sample Welch's *t* test).

Figure 3

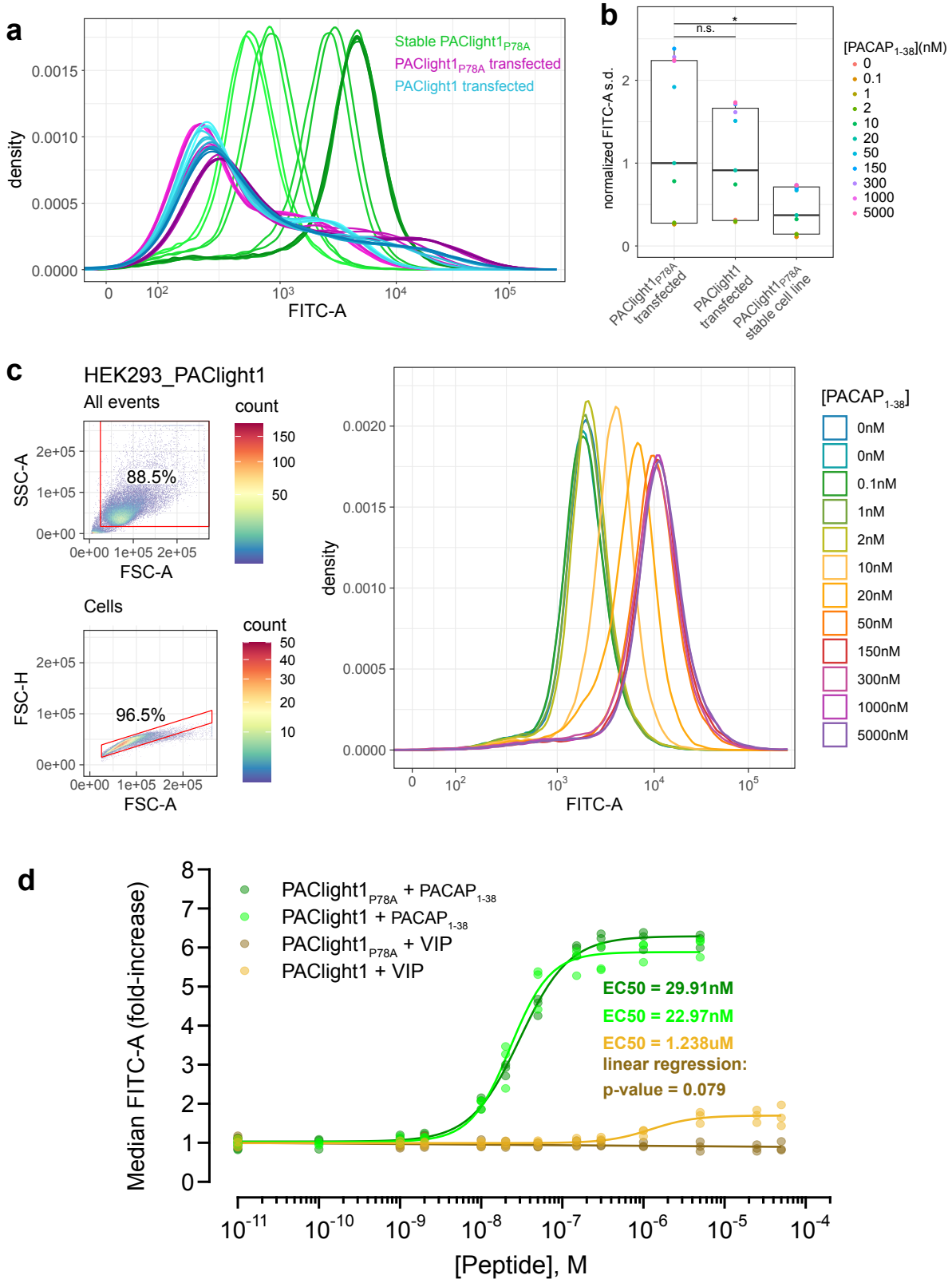
a
Stable PAClight1P78A
PAClight1P78A transfected
PAClight1 transfected
density
FITC-A
b
n.s.
*
normalized FITC-A s.d.
PAClight1P78A transfected
PAClight1 transfected
PAClight1P78A stable cell line
[PACAP1-38](nM)
0
0.1
1
2
10
20
50
150
300
1000
5000
c
HEK293_PAClight1
All events
count
SSC-A
FSC-A
88.5%
Cells
FSC-H
96.5%
density
FITC-A
[PACAP1-38]
0nM
0nM
0.1nM
1nM
2nM
10nM
20nM
50nM
150nM
300nM
1000nM
5000nM
d
PAClight1P78A + PACAP1-38
PAClight1 + PACAP1-38
PAClight1P78A + VIP
PAClight1 + VIP
EC50 = 29.91nM
EC50 = 22.97nM
EC50 = 1.238uM
linear regression:
p-value = 0.079
Median FITC-A (fold-increase)
[Peptide], M

827

Figure 3 | Comparison between transient and stable PAClight1$_{P78A}$ expression

a) A direct flow cytometric comparison between transfected HEK293T cells and stable and inducible HEK293_PAClight1$_{P78A}$ cells highlights the improved homogeneity of the distribution of expression levels in the newly generated stable cell line. Note the increased number of cells on both the low and high extremes in the transfected populations over the stable cell line population. Data from a full PACAP$_{1-38}$ titration series for each condition is presented. The overall variability in expression levels in the PAClight1$_{P78A}$- and PAClight1-transfected condition is very similar. **b)** The standard deviation of each density curve (normalized to the median standard deviation of the transfected PAClight1$_{P78A}$ condition) is plotted by condition and concentration. The median standard deviation of the stable HEK293_PAClight1$_{P78A}$ condition is reduced to only 37.4% of the transfected PAClight1$_{P78A}$ condition (Dunnett's test p= 0.0142). The median standard deviation varies little between transfected PAClight1$_{P78A}$ and PAClight1 cells (8.6% lower in PAClight1, Dunnett's test p= 0.5966). **c)** A representative example of a PACAP$_{1-38}$ titration series on stable HEK293_PAClight1 cells. Top left: Gating strategy used to gate cells by the area of the side scatter (SSC-A) vs. the area of the forward scatter (FSC-A). Bottom left: Gating strategy used to gate singlets (within the cells gate) by the height of the forward scatter (FSC-H) vs. the FSC-A. Right: Density curves of the FITC-A channel obtained from the singlet gate. **d)** Dose-response curves obtained from VIP and PACAP$_{1-38}$ titrations on stable HEK293_PAClight1$_{P78A}$ and stable HEK293_PAClight1 cells. PAClight1$_{P78A}$ and PAClight1 both have high affinities for PACAP$_{1-38}$ (PAClight1$_{P78A}$ EC50 = 29.91nM, PAClight1 EC50 = 22.97nM, n=3). While PAClight1 still shows a response to higher concentrations of VIP (EC50 = 1.24μM), PAClight1$_{P78A}$'s response to VIP is completely abolished up to concentrations of 50μM VIP ($F_{(1, 33)}$ = 3.28, p= 0.079, adj. R2= 0.06). Data in **a-c)** is derived from 100K original events recorded for each concentration and construct. Data in **d)** is derived from 100K recorded events across n=3 of each titration series.

Figure 4

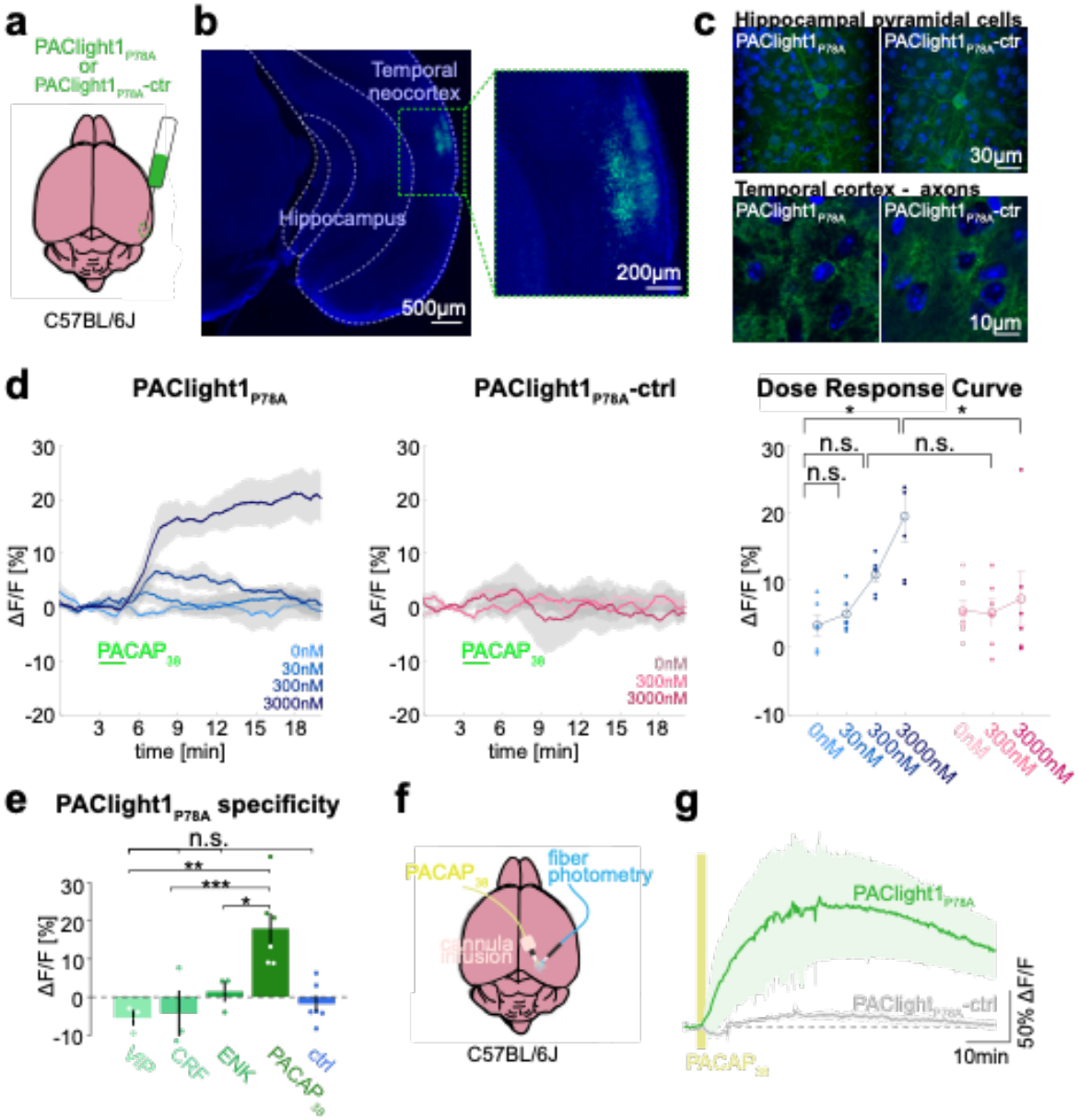
a
PAClight1P78A or PAClight1P78A-ctr
C57BL/6J
b
Temporal neocortex
Hippocampus
500µm
200µm
c
Hippocampal pyramidal cells
PAClight1P78A
PAClight1P78A-ctr
30µm
Temporal cortex - axons
10µm
d
PAClight1P78A
PAClight1P78A-ctrl
Dose Response Curve
ΔF/F [%]
time [min]
PACAP38
0nM
30nM
300nM
3000nM
n.s.
e
PAClight1P78A specificity
VIP
CRF
ENK
PACAP38
ctrl
f
fiber photometry
cannula infusion
C57BL/6J
g
PAClight1P78A
PAClight1P78A-ctrl
50% ΔF/F
10min

Figure 4 | Ex vivo and in vivo sensor characterization in mice

a) AAVs encoding the PAClight1$_{P78A}$ or PAClight1$_{P78A}$-ctrl sensor were injected into the temporal neocortex of adult mice. **b)** Representative epifluorescent image of PAClight1$_{P78A}$ fluorescence after 4 weeks of expression time. **c)** Maximum intensity projections of exemplary confocal images of PAClight1$_{P78A}$ and PAClight1$_{P78A}$-ctrl-expressing neurons and neuropil in hippocampus and cortex enhanced with GFP-immunostaining and counterstained with DAPI (blue). **d)** Acute mouse brain slices expressing PAClight1$_{P78A}$ (left) and PAClight1$_{P78A}$-ctrl (middle) were used to test the sensitivity of the sensor in the mammalian brain. PACAP$_{1-38}$ was bath-applied for 2min (green bar) at indicated concentrations. Data shown as mean ± standard error of the mean (SEM). *N*=6 slices per condition from ≥3 mice. Right: Dose-response curve for PAClight1$_{P78A}$ $\Delta F/F_0$ (blue shades) and PAClight1$_{P78A}$-ctrl $\Delta F/F_0$ (pink shades) in response to indicated concentrations of PACAP$_{1-38}$. Mann-Whitney-U-tests with Bonferroni corrections revealed no statistically significant difference in mean PAClight1$_{P78A}$ peak responses to bath-application of 30nM (p=2.909), and 300nM PACAP$_{1-38}$ (p=0.0519) compared to 0nM PACAP$_{1-38}$. We found a significant difference between 0nM and 3000nM PACAP$_{1-38}$ (p=0.013). Comparing mean peak $\Delta F/F_0$ PAClight1$_{P78A}$ responses with PAClight1$_{P78A}$-ctrl revealed a significant difference when bath-applying 3000nM (p=0.041), but not for 300nM (p=0.084). **e)** Quantification of mean PAClight1$_{P78A}$ peak responses to bath-application of 3µM VIP, CRF, ENK, PACAP$_{1-38}$ and negative control (ctrl) in acute mouse brain slices. *N*=3-6 slices per condition from ≥3 mice. No statistically significant difference ($F_{(4,10)}$=5.15) was found between ctrl and VIP (p=0.9705), ctrl and CRF (p=0.9937) and ctrl and ENK (p=0.9726). A statistically significant difference ($F_{(3,8)}$=9.19) was detected between PACAP$_{1-38}$ and VIP (p=0.007), PACAP$_{1-38}$ and CRF (p=0.001) and PACAP$_{1-38}$ and ENK (p=0.045). Statistically significant differences are indicated with an asterisk, non-significant differences with n.s. **f)** AAVs encoding the PAClight1$_{P78A}$ or PAClight1$_{P78A}$-ctrl sensor were injected into the neocortex of adult mice. Fiberoptic cannulae and acute microinfusion cannulae were implanted nearby. **g)** PAClight1$_{P78A}$ and PAClight1$_{P78A}$-ctrl fluorescence changes upon microinfusion of 300µM PACAP$_{1-38}$ (200nl) recorded with fiber photometry in freely behaving mice. *N*=2 mice each. Data shown as mean ± SEM.

Figure 5

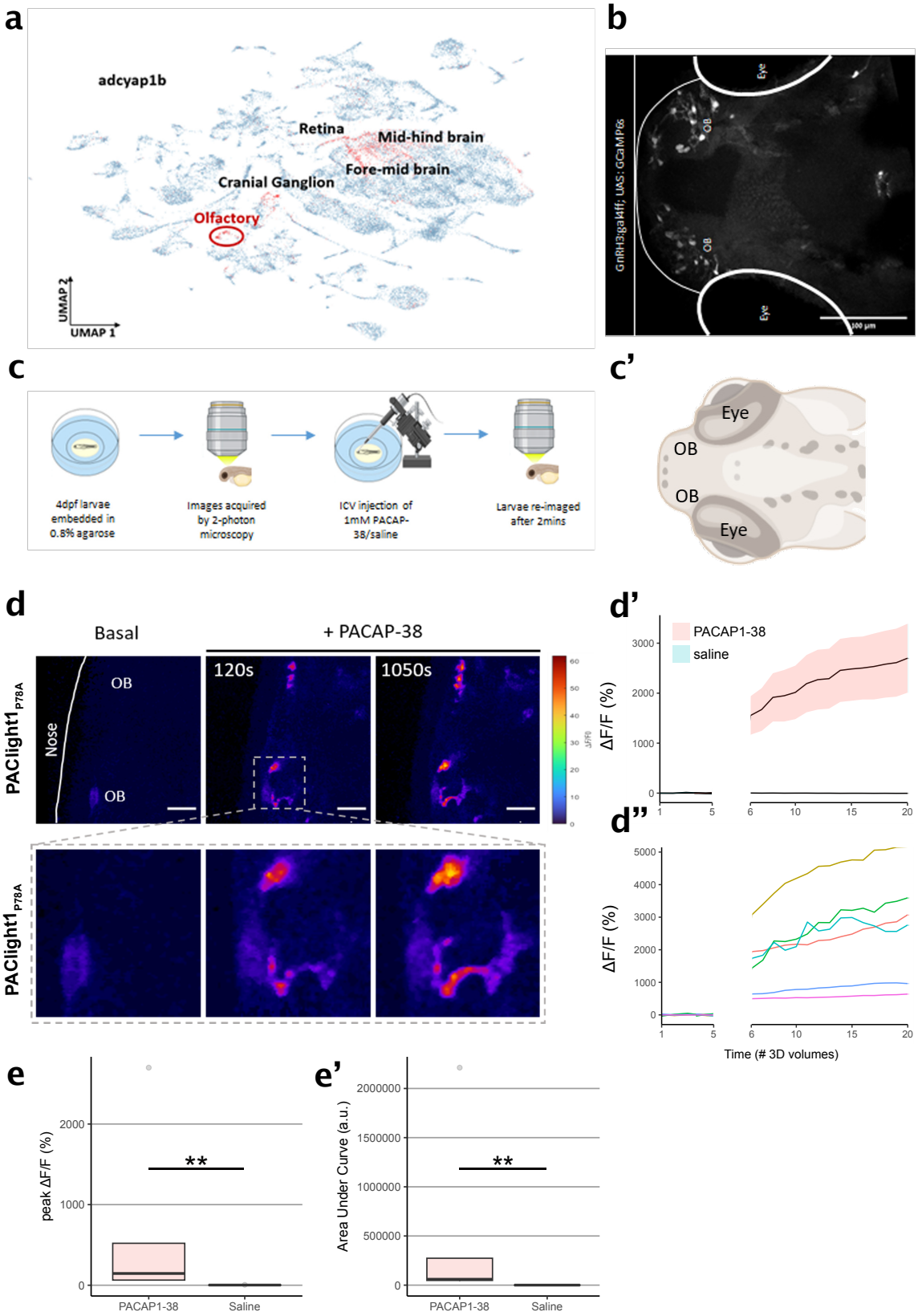
a
adcyap1b
Retina
Mid-hind brain
Fore-mid brain
Cranial Ganglion
Olfactory
UMAP 2
UMAP 1
b
Eye
OB
OB
Eye
GnRH3:gal4ff; UAS:GCaMP6s
100 µm
c
4dpf larvae embedded in 0.8% agarose
Images acquired by 2-photon microscopy
ICV injection of 1mM PACAP-38/saline
Larvae re-imaged after 2mins
c'
Eye
OB
OB
Eye
d
Basal
+ PACAP-38
120s
1050s
OB
Nose
OB
PAClight1P78A
PAClight1P78A
ΔF/F
d'
PACAP1-38
saline
ΔF/F (%)
d''
ΔF/F (%)
Time (# 3D volumes)
e
peak ΔF/F (%)
**
PACAP1-38
Saline
e'
Area Under Curve (a.u.)
**
PACAP1-38
Saline

897

Figure 5 | Characterization of PAClight1 in live zebrafish larvae

a) Uniform manifold approximation and projection (UMAP) showing topological distribution of single cell gene expression clusters with high adcyap1b (PACAP) expression of 0-4 dpf larvae. High adcyap1b expression is highlighted in the olfactory bulb. **b)** Maximum intensity projection image of the 4dpf *Tg(GnRH3:gal4ff; UAS:GCaMP6s)* larvae shows GnRH3 expressing cells in the olfactory bulb. **c)** Schema representing the experimental design. 4dpf larvae were immobilized and 3D volumetric images across time were obtained during the naïve state. 50nl of 1mM PACAP-38/saline was injected intracerebroventricularly and the same larvae was imaged again after 2mins. **c')** Schema of imaged region of interest including the olfactory bulb in the 4dpf larvae. **d)** (top) Representative maximum intensity projection of two-photon volumetric images showing naïve sensor at baseline and its increase in fluorescence after PACAP-38 injection in the same larvae along time (scale bar = 20um). Colour bar is representative of the $\Delta F/F_0$ in the images. (bottom) Zoomed-in image of the left olfactory bulb showing increase in fluorescence after injection of $PACAP_{1-38}$. **d')** Representative quantification of the change in fluorescence with respect to basal fluorescence depicted as $\Delta F/F_0$. $PACAP_{1-38}$injected larvae show an increase in activity of the fluorescent sensor as compared to their saline injected sibling controls. **d'')** Individual cell traces show variability in sensor responses in different cells that may be a function of expression of the sensor on the cell surface. **e,e')** Peak $\Delta F/F_0$ and Area under the Curve (AUC) of $PACAP_{1-38}$injected larvae is significantly higher than the saline injected controls ($n_{control}$ =5, $n_{PACAP-38}$ =5, Kolmogorov-Smirnov test p=0.0079)

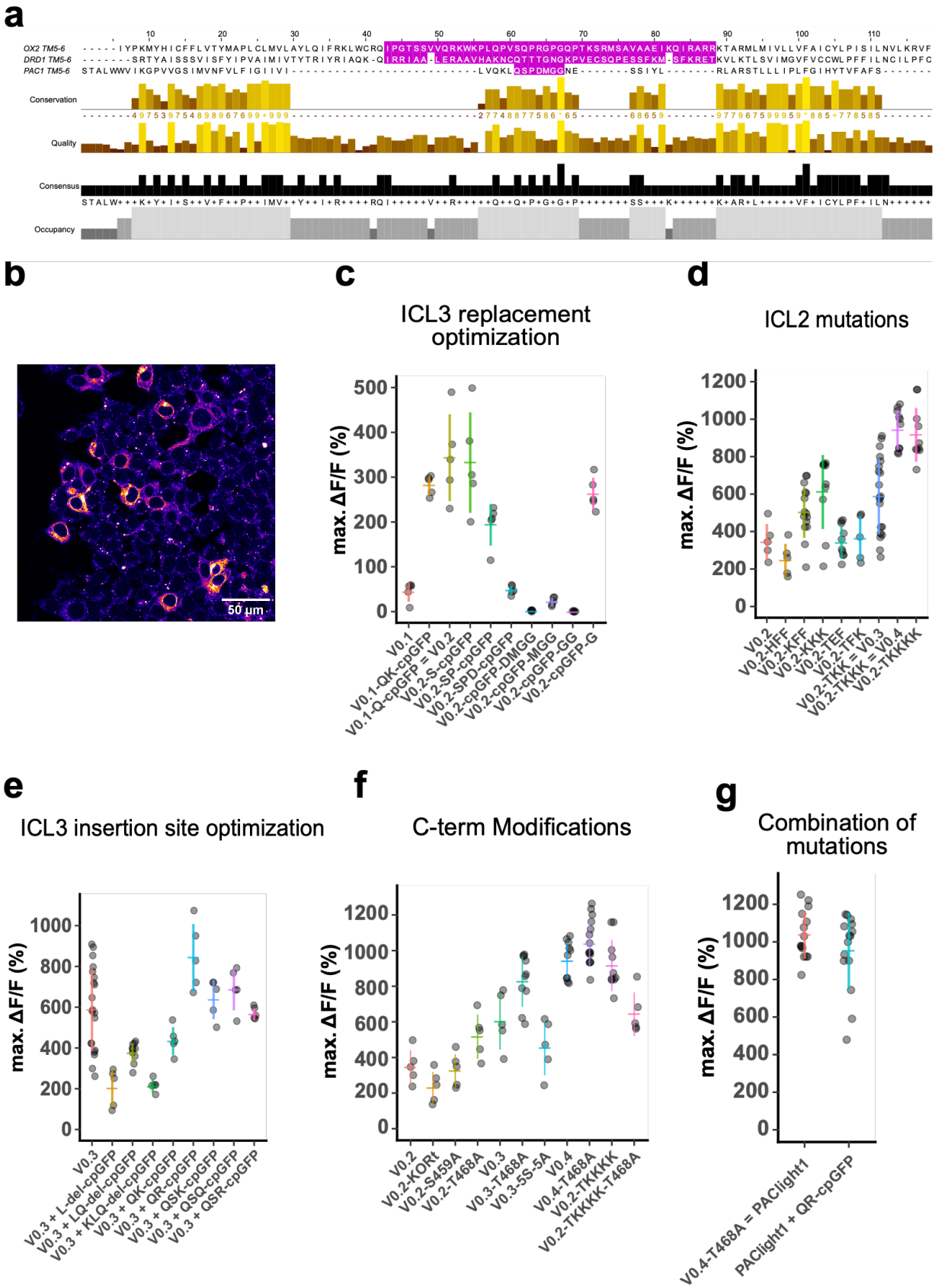
a
OX2 TM5-6
DRD1 TM5-6
PAC1 TM5-6
Conservation
Quality
Consensus
Occupancy
b
50 µm
c
ICL3 replacement optimization
max. ΔF/F (%)
V0.1
V0.1-QK-cpGFP
V0.1-Q-cpGFP = V0.2
V0.2-S-cpGFP
V0.2-SP-cpGFP
V0.2-SPD-cpGFP
V0.2-cpGFP-DMGG
V0.2-cpGFP-MGG
V0.2-cpGFP-GG
V0.2-cpGFP-G
d
ICL2 mutations
max. ΔF/F (%)
V0.2
V0.2-HFF
V0.2-KFF
V0.2-KKK
V0.2-TEF
V0.2-TFK
V0.2-TKK = V0.3
V0.2-TKKK = V0.4
V0.2-TKKKK
e
ICL3 insertion site optimization
max. ΔF/F (%)
V0.3
V0.3 + L-del-cpGFP
V0.3 + LQ-del-cpGFP
V0.3 + KLQ-del-cpGFP
V0.3 + QK-cpGFP
V0.3 + QR-cpGFP
V0.3 + QSK-cpGFP
V0.3 + QSQ-cpGFP
V0.3 + QSR-cpGFP
f
C-term Modifications
max. ΔF/F (%)
V0.2
V0.2-KORt
V0.2-S459A
V0.2-T468A
V0.3
V0.3-T468A
V0.3-5S-5A
V0.4
V0.4-T468A
V0.2-TKKKK
V0.2-TKKKK-T468A
g
Combination of mutations
max. ΔF/F (%)
V0.4-T468A = PAClight1
PAClight1 + QR-cpGFP

920

Extended Data Figure 1| Optimizing the fluorescent response of PAClight sensors

a) Multiple amino acid sequence alignment of the TM5, ICL3, and TM6 domains of the human orexin 2 receptor (OX2), the human D1 dopamine receptor (DRD1), and of the human PAC1Rnull (PAC1). The sequences replaced by the cpGFP module in the OxLight1, dLight1.3b, and PAClight1$_{P78A}$ sensors are highlighted in magenta. The OX2 and DRD1 receptor sequences align well due to the fact that they both belong to the class A GPCRs. The PAC1Rnull belongs to the class B1 family of GPCRs and hence aligns less well to the OX2 and DRD1 backbones. We therefore guided the initial design and site of cpGFP module insertion by protein structure rather than by amino acid sequence. **b)** Pseudo-colored confocal micrograph of HEK293T cells expressing the prototypical PAClight_V0.1. Plasma membrane expression can be detected, but a significant amount of sensor protein is retained intracellularly. **c)** Scatterplot representing insertion site variants screened for maximum dynamic range. Reinsertion of the glutamine on the N-terminal side of the cpGFP module (PAClight_V0.2) drastically increased the dynamic range to 343% $\Delta F/F_0$ (compared to 43.4% $\Delta F/F_0$ in PAClight_V0.1). **d)** Point mutations in the intracellular loop 3 (ICL3) further improved the dynamic range to 588% $\Delta F/F_0$ for PAClight_V0.3 (point mutations: F259K/F260K) and to 942% $\Delta F/F_0$ for PAClight_V0.4 (point mutations: F259K/F260K /P261K). **e)** On the backbone of the improved ICL2 variant PAClight_V0.3 we screened again for the optimal insertion site of the cpGFP module. To this end we performed serial deletions as well as insertions of charged residues on the residues n-terminal to the cpGFP module. This small-scale screen identified a mutant with a glutamine and arginine insertion before the cpGFP module (PAClight_V0.3+QR-cpGFP) with improved dynamic range ($\Delta F/F_0$ = 844%) compared to the PAClight_V0.3 backbone. **f)** To abolish β-Arrestin recruitment and further improve membrane localization, we further screened C-terminus mutants. We included mutants in this screen in which we replaced the C-terminus with the tail of the kappa opioid receptor (KORt), as well as point mutants of known post-translational modification sites and serine residues. The point mutation of the T468 to alanine further improved plasma membrane localization (data not shown) and improved the dynamic range from 942% $\Delta F/F_0$ (in PAClight_V0.4) to 1037% $\Delta F/F_0$. The resulting construct was named PAClight1. **g)** Since the insertion of QR in front of the cpGFP module had a positive effect on dynamic range on the backbone of PAClight_V0.3 **(e)**, we also tested this insertion of QR on the PAClight1 backbone. However, the QR insertion did not yield improved dynamic range on the PAClight1 backbone ($\Delta F/F_0$ = 953%) and was hence rejected. Each datapoint represents the average of the max$\Delta F/F_0$ within one ROI. In each replicate 5 ROIs each were quantified. *N*=4 for V0.3. *n*=3 for V0.2_KFF, PAClight1, and PAClight1+QR-cpGFP. *n*=2 for V0.2_KKK, V0.2_TEF, V0.2_KKKK, V0.3_LQ-del-cpGFP, V0.3_T468A, and V0.4. For all other constructs *n*=1 replicates each was screened. The y-axis position of the colored horizontal bars represents the mean across all replicates within a construct. The extent of the colored vertical bars represents +/- 1 standard deviation. For ease of comparability some constructs are potted on multiple plots.

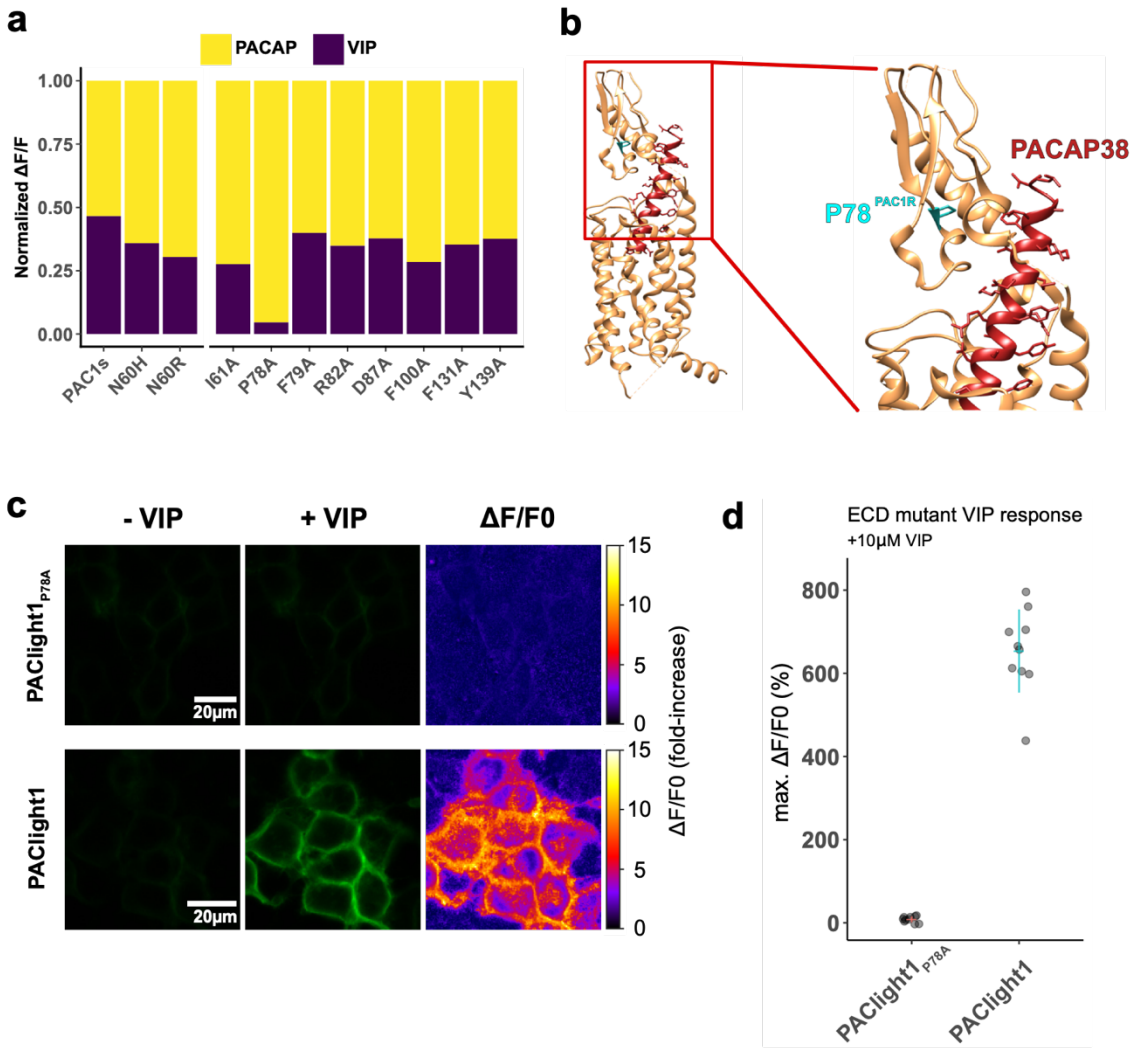

Extended Data Figure 2| Engineering PACAP selectivity in PAClight1$_{P78A}$
a) Stacked bar plot demonstrating the relative fluorescent response of ECD mutants towards 500nM of VIP followed by 9.09µM PACAP$_{1-38}$. The mutant PAC1s contains the naturally occurring splice mutation (deletion) on the ECD. The N60H and N60R were inspired by the analysis of protein structure. The remaining alanine point mutants (right side of bar plot) were inspired by molecular dynamics (see main text). The P78A point mutation on the ECD resulted in excellent improvement of specificity. The highly PACAP-specific mutant was named PAClight1$_{P78A}$. The data is normalized to the maximum response within each condition. *n*=1 for each mutant. **b)** Visualization of the ECD mutation P78A (cyan) on the backbone of a previously published cryo-EM structure of PAC1Rnull (beige) in interaction with PACAP$_{1-38}$ (dark red) (PDB: 6LPB)[22]. **c)** Representative confocal micrographs of HEK293T cells expressing the PACAP-specific PAClight1$_{P78A}$ and the VIP-responsive PAClight1 sensors before (left) and after (middle) 10µM VIP bath application. Pixel-wise calculation of $\Delta F/F_0$ is shown on the right. Note the complete absence of a fluorescent response to VIP in the PAClight1$_{P78A}$ mutant. **d)** Quantification of the averaged maximum dynamic range of PAClight1$_{P78A}$ ($\Delta F/F_0$ = 8.28%) vs. PAClight1 ($\Delta F/F_0$ = 654%) in response to 10µM VIP.

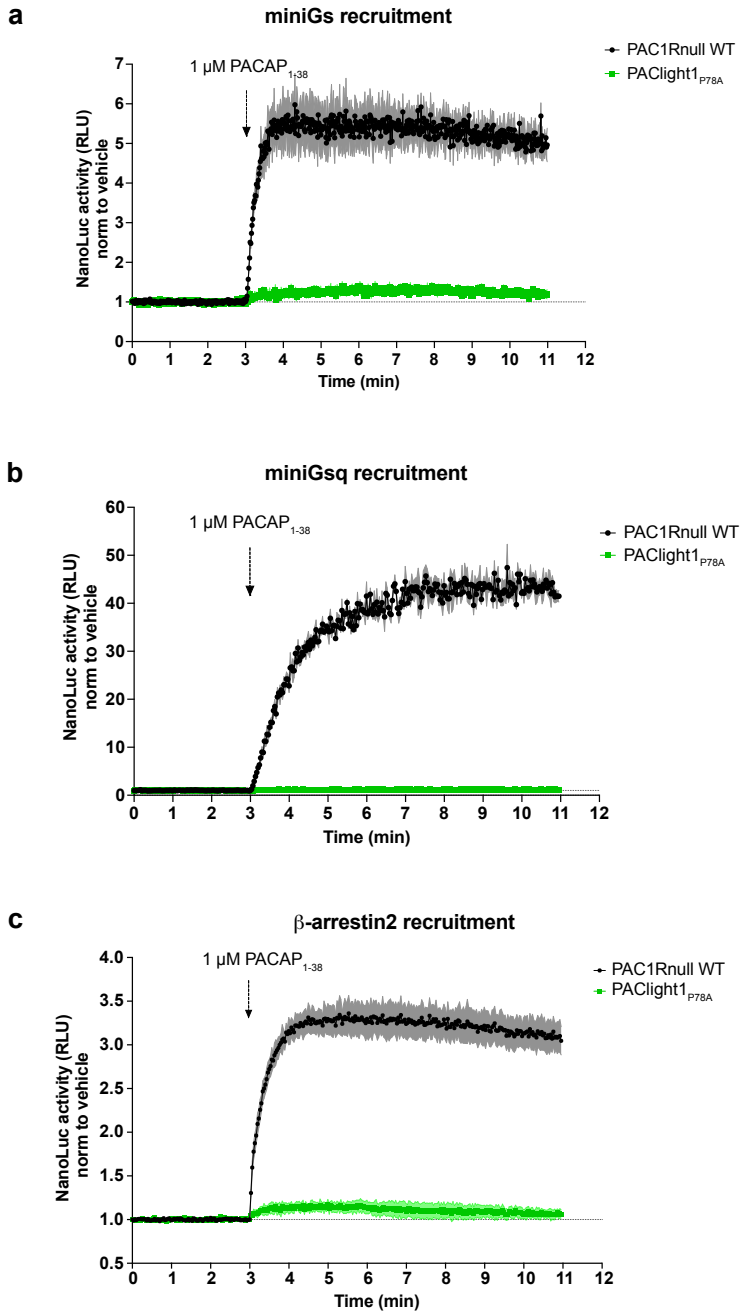

984
985
986 **Extended Data Figure 3| Characterization of PAClight1$_{P78A}$ coupling to transducer**
987 **proteins**
988 NanoLuc complementation assays were employed to measure the ability of human SmBiT-
989 PAC1R or SmBiT-PAClight1$_{P78A}$ to recruit LgBiT-miniGs (a), -miniGsq (b) or -β-arrestin2 (c) in an
990 agonist-induced manner. Luminescence emission (relative luminescence units, RLU) was
991 monitored during application of agonist (PACAP$_{1-38}$) and was normalized to control cells with
992 application of buffer (vehicle). Dots represent average datapoints, shades represent SEM. n=3
993 for each condition.
994

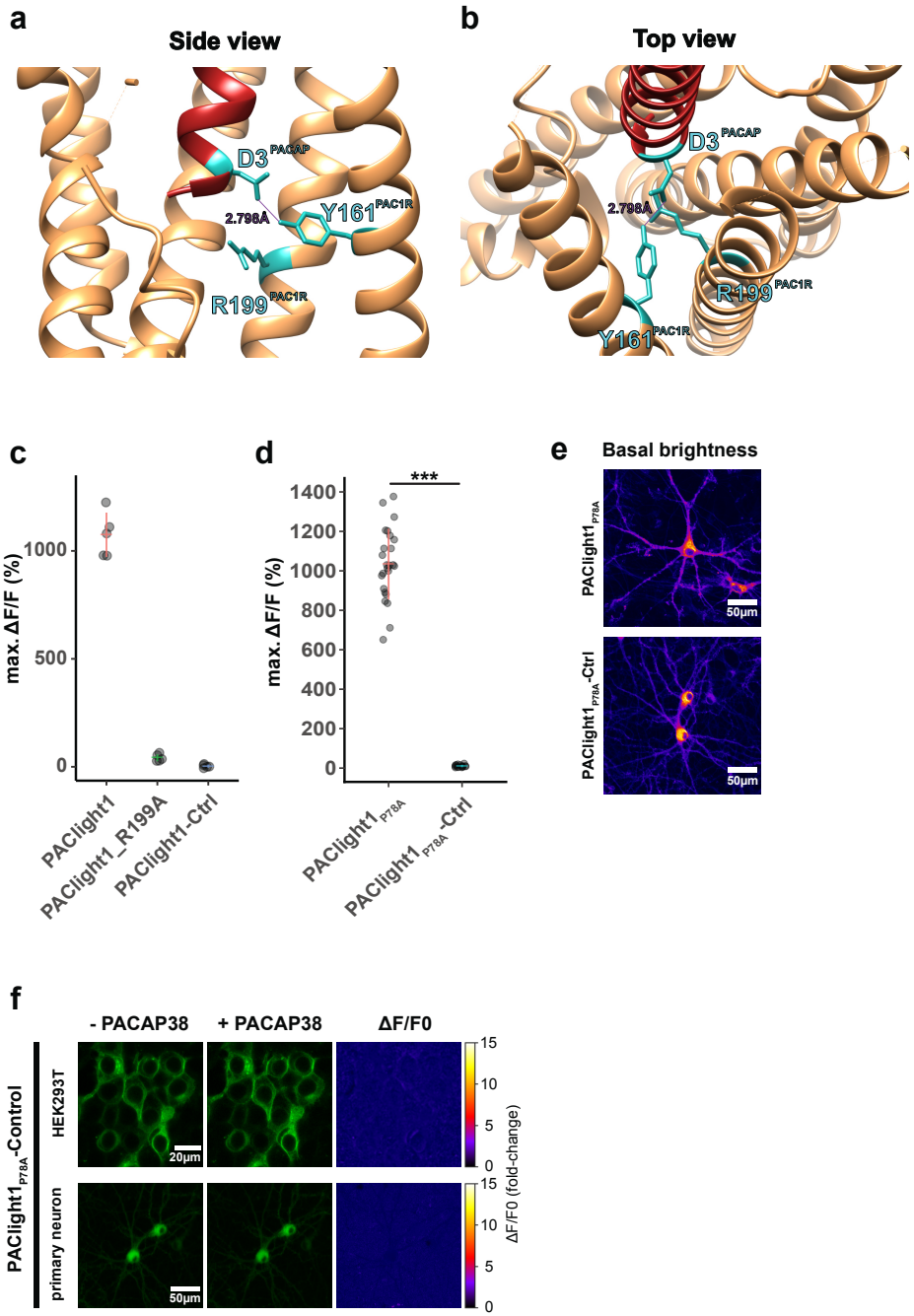
a
Side view
D3 PACAP
2.798Å
Y161 PAC1R
R199 PAC1R
b
Top view
D3 PACAP
2.798Å
R199 PAC1R
Y161 PAC1R
c
max. ΔF/F (%)
1000
500
0
PAClight1
PAClight1_R199A
PAClight1-Ctrl
d
max. ΔF/F (%)
1400
1200
1000
800
600
400
200
0
***
PAClight1 P78A
PAClight1 P78A -Ctrl
e
Basal brightness
PAClight1 P78A
PAClight1 P78A -Ctrl
50μm
50μm
f
- PACAP38
+ PACAP38
ΔF/F0
PAClight1 P78A -Control
HEK293T
primary neuron
20μm
50μm
15
10
5
0
ΔF/F0 (fold-change)

995

Extended Data Figure 4| Development of a PAClight1$_{P78A}$-ctrl sensor

a) Side view of the protein structure of the hmPAC1R transmembrane domain (beige) in interaction with PACAP$_{1-38}$ (red). Residues Y161 and R199 of the hmPAC1R, as well as residue D3 of PACAP are highlighted in cyan. The hydrogen bond between D3 and Y161 is indicated with a dashed line. **b)** Top view onto the same protein structures depicted in **a)**. **c)** Maximum dynamic range of HEK293T cells expressing PAClight1 (mean= 1075% $\Delta F/F_0$), PAClight1_R199A (mean= 41.9% $\Delta F/F_0$), and PAClight1-ctrl (mean= 2.87% $\Delta F/F_0$). **d)** Maximum dynamic range of HEK293T cells expressing PAClight1$_{P78A}$ (mean= 1034% $\Delta F/F_0$) and PAClight1$_{P78A}$-ctrl (mean= 10.44% $\Delta F/F_0$). **e)** Comparison of basal brightness levels of PAClight1$_{P78A}$ and PAClight1$_{P78A}$-ctrl expressed in rat primary neurons via viral transduction. **f)** Representative examples of PAClight1$_{P78A}$-ctrl expressed in HEK293T cells (top row) and rat primary neurons (bottom row) before (left column) and after (middle column) bath application of 10µM PACAP$_{1-38}$. The right column depicts the pixel-wise calculated $\Delta F/F_0$. No detectable increase in fluorescence is observed.

1013

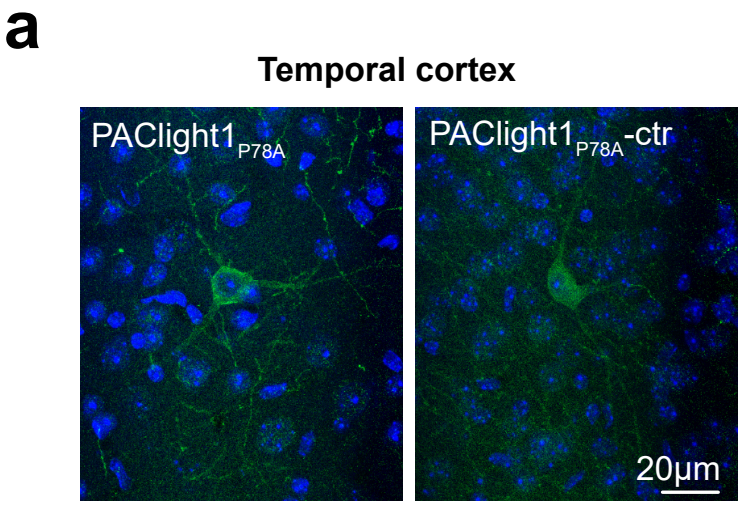

1014
1015
1016 **Extended Data Figure 5| Validation of PAClight1$_{P78A}$ and PAClight1$_{P78A}$-ctrl sensors in**
1017 **mammalian brains**
1018 Maximum intensity projections of exemplary confocal images of PAClight1$_{P78A}$ and
1019 PAClight1$_{P78A}$-ctrl-expressing neurons in the cortex enhanced with immunostaining and
1020 counterstained with DAPI (blue).

References

1. Top Pharmaceuticals Poster | Njarðarson. https://njardarson.lab.arizona.edu/content/top-pharmaceuticals-poster.
2. Peptide Therapeutics Market. https://www.transparencymarketresearch.com/peptide-therapeutics-market.html.
3. Wang, L. *et al.* Therapeutic peptides: current applications and future directions. *Sig Transduct Target Ther* **7**, 1–27 (2022).
4. Johnson, G. C., Parsons, R., May, V. & Hammack, S. E. The Role of Pituitary Adenylate Cyclase-Activating Polypeptide (PACAP) Signaling in the Hippocampal Dentate Gyrus. *Front. Cell. Neurosci.* **14**, (2020).
5. Dickson, L. & Finlayson, K. VPAC and PAC receptors: From ligands to function. *Pharmacology & Therapeutics* **121**, 294–316 (2009).
6. Hashimoto, H. *et al.* Distribution of the mRNA for a pituitary adenylate cyclase-activating polypeptide receptor in the rat brain: An in situ hybridization study. *Journal of Comparative Neurology* **371**, 567–577 (1996).
7. Condro, M. C. *et al.* High-resolution characterization of a PACAP-EGFP transgenic mouse model for mapping PACAP-expressing neurons. *Journal of Comparative Neurology* **524**, 3827–3848 (2016).
8. *Pituitary Adenylate Cyclase Activating Polypeptide — PACAP*. vol. 11 (Springer International Publishing, Cham, 2016).
9. Blechman, J. & Levkowitz, G. Alternative Splicing of the Pituitary Adenylate Cyclase-Activating Polypeptide Receptor PAC1: Mechanisms of Fine Tuning of Brain Activity. *Front Endocrinol (Lausanne)* **4**, 55 (2013).
10. Biran, J. *et al.* Splice-specific deficiency of the PTSD-associated gene PAC1 leads to a paradoxical age-dependent stress behavior. *Sci Rep* **10**, 9559 (2020).
11. Patriarchi, T. *et al.* Ultrafast neuronal imaging of dopamine dynamics with designed genetically encoded sensors. *Science* **360**, eaat4422 (2018).
12. Patriarchi, T. *et al.* An expanded palette of dopamine sensors for multiplex imaging in vivo. *Nat Methods* **17**, 1147–1155 (2020).
13. Patriarchi, T. *et al.* Imaging neuromodulators with high spatiotemporal resolution using genetically encoded indicators. *Nat Protoc* **14**, 3471–3505 (2019).
14. Sun, F. *et al.* A Genetically Encoded Fluorescent Sensor Enables Rapid and Specific Detection of Dopamine in Flies, Fish, and Mice. *Cell* **174**, 481-496.e19 (2018).
15. Peng, W. *et al.* Regulation of sleep homeostasis mediator adenosine by basal forebrain glutamatergic neurons. *Science* **369**, (2020).
16. Oe, Y. *et al.* Distinct temporal integration of noradrenaline signaling by astrocytic second messengers during vigilance. *Nat Commun* **11**, 1–15 (2020).
17. Duffet, L. *et al.* A genetically encoded sensor for in vivo imaging of orexin neuropeptides. *Nat Methods* **19**, 231–241 (2022).
18. Duffet, L. *et al.* Optical tools for visualizing and controlling human GLP-1 receptor activation with high spatiotemporal resolution. 2023.02.14.528498 Preprint at https://doi.org/10.1101/2023.02.14.528498 (2023).
19. Kagiampaki, Z. *et al.* Sensitive multicolor indicators for monitoring norepinephrine in vivo. *Nat Methods* 1–11 (2023) doi:10.1038/s41592-023-01959-z.
20. Wang, H. *et al.* A toolkit of highly selective and sensitive genetically encoded neuropeptide sensors. 2022.03.26.485911 Preprint at https://doi.org/10.1101/2022.03.26.485911 (2022).
21. Hornbeck, P. V., Chabra, I., Kornhauser, J. M., Skrzypek, E. & Zhang, B. PhosphoSite: A bioinformatics resource dedicated to physiological protein phosphorylation. *PROTEOMICS* **4**, 1551–1561 (2004).
22. Kobayashi, K. *et al.* Cryo-EM structure of the human PAC1 receptor coupled to an engineered heterotrimeric G protein. *Nat Struct Mol Biol* **27**, 274–280 (2020).
23. Liao, C., Remington, J. M., May, V. & Li, J. Molecular Basis of Class B GPCR Selectivity for the Neuropeptides PACAP and VIP. *Frontiers in Molecular Biosciences* **8**, (2021).
24. Duffet, L. *et al.* Optical tools for visualizing and controlling human GLP-1 receptor activation with high spatiotemporal resolution. *eLife* https://elifesciences.org/articles/86628/figures (2023) doi:10.7554/eLife.86628.

25. Lerner, E. A., Iuga, A. O. & Reddy, V. B. Maxadilan, a PAC1 receptor agonist from sand flies. *Peptides* **28**, 1651–1654 (2007).
26. A Neuropeptide Gene Defined by the Drosophila Memory Mutant amnesiac. https://www.science.org/doi/10.1126/science.7754370 doi:10.1126/science.7754370.
27. Doan, N.-D. *et al.* Design and in vitro characterization of PAC1/VPAC1-selective agonists with potent neuroprotective effects. *Biochemical Pharmacology* **81**, 552–561 (2011).
28. Bourgault, S. *et al.* Molecular and Conformational Determinants of Pituitary Adenylate Cyclase-Activating Polypeptide (PACAP) for Activation of the PAC1 Receptor. *J. Med. Chem.* **52**, 3308–3316 (2009).
29. Klein Herenbrink, C. *et al.* Multimodal detection of dopamine by sniffer cells expressing genetically encoded fluorescent sensors. *Commun Biol* **5**, 1–9 (2022).
30. Cauvin, A. *et al.* The novel VIP-like hypothalamic polypeptide PACAP interacts with high affinity receptors in the human neuroblastoma cell line NB-OK. *Peptides* **11**, 773–777 (1990).
31. Buscail, L. *et al.* Presence of highly selective receptors for PACAP (pituitary adenylate cyclase activating peptide) in membranes from the rat pancreatic acinar cell line AR 4-2J. *FEBS Letters* **262**, 77–81 (1990).
32. Zhang, L. *et al.* Behavioral role of PACAP signaling reflects its selective distribution in glutamatergic and GABAergic neuronal subpopulations. *Elife* **10**, e61718 (2021).
33. Loryan, I., Fridén, M. & Hammarlund-Udenaes, M. The brain slice method for studying drug distribution in the CNS. *Fluids and Barriers of the CNS* **10**, 6 (2013).
34. MacRae, C. A. & Peterson, R. T. Zebrafish as tools for drug discovery. *Nat Rev Drug Discov* **14**, 721–731 (2015).
35. Zon, L. I. & Peterson, R. T. In vivo drug discovery in the zebrafish. *Nat Rev Drug Discov* **4**, 35–44 (2005).
36. Sturtzel, C. *et al.* Refined high-content imaging-based phenotypic drug screening in zebrafish xenografts. *npj Precis. Onc.* **7**, 1–16 (2023).
37. Amir-Zilberstein, L. *et al.* Homeodomain protein otp and activity-dependent splicing modulate neuronal adaptation to stress. *Neuron* **73**, 279–291 (2012).
38. Farrell, J. A. *et al.* Single-cell reconstruction of developmental trajectories during zebrafish embryogenesis. *Science* **360**, eaar3131 (2018).
39. Farnsworth, D. R., Saunders, L. M. & Miller, A. C. A single-cell transcriptome atlas for zebrafish development. *Developmental Biology* **459**, 100–108 (2020).
40. Laschet, C., Dupuis, N. & Hanson, J. A dynamic and screening-compatible nanoluciferase-based complementation assay enables profiling of individual GPCR–G protein interactions. *Journal of Biological Chemistry* **294**, 4079–4090 (2019).
41. Mirdita, M. *et al.* ColabFold: making protein folding accessible to all. *Nat Methods* 1–4 (2022) doi:10.1038/s41592-022-01488-1.
42. Sievers, F. & Higgins, D. G. Clustal Omega, accurate alignment of very large numbers of sequences. *Methods Mol. Biol.* **1079**, 105–116 (2014).
43. Waterhouse, A. M., Procter, J. B., Martin, D. M. A., Clamp, M. & Barton, G. J. Jalview Version 2--a multiple sequence alignment editor and analysis workbench. *Bioinformatics* **25**, 1189–1191 (2009).
44. Hartrampf, N. *et al.* Synthesis of proteins by automated flow chemistry. *Science* **368**, 980–987 (2020).
45. Wan, Q. *et al.* Mini G protein probes for active G protein–coupled receptors (GPCRs) in live cells. *J. Biol. Chem.* **293**, 7466–7473 (2018).
46. Kawakami, K. Tol2: a versatile gene transfer vector in vertebrates. *Genome Biology* **8**, S7 (2007).
47. Golan, M. *et al.* Synaptic communication mediates the assembly of a self-organizing circuit that controls reproduction. *Sci Adv* **7**, eabc8475 (2021).
48. Edelstein, A. D. *et al.* Advanced methods of microscope control using μManager software. *Journal of Biological Methods* **1**, e10–e10 (2014).
49. Melzer, S. *et al. Bombesin-like Peptide Recruits Disinhibitory Cortical Circuits and Enhances Fear Memories*. http://biorxiv.org/lookup/doi/10.1101/2020.10.26.355123 (2020) doi:10.1101/2020.10.26.355123.
50. Jumper, J. *et al.* Highly accurate protein structure prediction with AlphaFold. *Nature* **596**, 583–589 (2021).